Doping dependent optical properties of $Bi_2Sr_2CaCu_2O_{8+\delta}$

2007 J. Phys.: Condens. Matter 19 125208

(http://iopscience.iop.org/0953-8984/19/12/125208)

IOP PUBLISHING JOURNAL OF PHYSICS: CONDENSED MATTER

J. Phys.: Condens. Matter **19** (2007) 125208 (32pp) doi:10.1088/0953-8984/19/12/125208

Doping dependent optical properties of $Bi_2Sr_2CaCu_2O_{8+\delta}$

J Hwang[1], T Timusk[1,2] and G D Gu[3]

[1] Department of Physics and Astronomy, McMaster University, Hamilton, ON, L8S 4M1, Canada
[2] The Canadian Institute of Advanced Research, Toronto, ON, M5G 1Z8, Canada
[3] Department of Physics, Brookhaven National Laboratory, Upton, NY 11973-5000, USA

E-mail: hwangjs@mcmaster.ca

Received 28 June 2006, in final form 29 October 2006
Published 6 March 2007
Online at stacks.iop.org/JPhysCM/19/125208

Abstract

We report on the *ab*-plane reflectance of the high temperature superconductor $Bi_2Sr_2CaCu_2O_{8+\delta}$ (Bi-2212). Measurements on samples spanning the doping range from underdoped with $T_c = 67$ K (UD), to optimally doped with $T_c = 96$ K (OPT), to overdoped with $T_c = 60$ K (OD) were made from room temperature down to the superconducting state regime. The measured reflectance data were analysed to extract the optical conductivity and the real and imaginary parts of the free carrier optical self-energy. We get an estimate of the dc resistivity from the low frequency extrapolation of the optical conductivity and the superfluid density from the imaginary part of the optical conductivity. The conductivity sum rule can be related to the changes of the kinetic energy of the system. When this system becomes a superconductor, the kinetic energy decreases in the underdoped samples and increases in the overdoped ones. The optical self-energy, obtained from the extended Drude model, is dominated by two channels of interaction: a sharp mode and a broad background. The amplitude of the mode is strongly doping and temperature dependent whereas the background decreases weakly with doping and is nearly temperature independent.

(Some figures in this article are in colour only in the electronic version)

1. Introduction

Since the discovery of high temperature superconductivity in the copper oxides [1] the dynamical properties of the charge carriers in these materials have been investigated with a variety of spectroscopic techniques. Within a certain class of theories these properties provide a direct fingerprint of the mechanism of superconductivity. For example, if analogously to the BCS superconductor case, superconductivity is driven by the exchange of bosons,

then a study of the self-energy spectrum of the superconducting current carriers would help us in identifying the relevant bosons. Traditionally this has been done with tunnelling spectroscopy where numerical inversion techniques using Migdal–Eliashberg theory [2] revealed spectroscopic fingerprints in the self-energy that could be compared with the phonon densities of states determined by inelastic neutron scattering and thereby unambiguously identified as phonons [3]. The self-energy spectra of the high temperature superconductors have also been investigated with increasing success with advanced spectroscopic techniques [4] including angle resolved photoemission (ARPES), tunnelling, optics and magnetic neutron scattering methods, but so far at least no consensus has been achieved in the interpretation of these spectra.

Contrasting with the traditional BCS mechanism of boson exchange there are alternative, exotic models of the mechanism of high temperature superconductivity involving the formation of new states at high temperature which would then Bose condense to form a superconductor as the temperature is lowered. There have also been suggestions that combine the two pictures where at low doping levels, close to the antiferromagnetic part of the phase diagram, an exotic mechanism operates but with increasing hole concentration a more conventional boson exchange takes over. To throw some light on these issues we have undertaken a study of the spectrum of excitations responsible for the self-energy of the carriers as a function of doping in the Bi-2212 system using the optical conductivity as our experimental probe. The Bi-2212 system has several advantages for such an investigation. First the system can be doped from the moderately underdoped region with $T_c = 60$ K through the optimally doped well into the overdoped region with $T_c = 60$ K. Furthermore, because the crystals of this material can be vacuum cleaved, they have also been studied extensively with ARPES [5] and tunnelling [6].

The extended Drude model that we use to find the real and imaginary parts of the scattering rate and the self-energy assumes that there is only one channel of conductivity and that any deviation from the Drude form is due to inelastic interactions. The validity of this assumption can be tested to some extent by comparing the scattering rate obtained from optics with the results from ARPES in the nodal direction. When such comparisons are made the resulting self-energy spectra generally agree to an accuracy of about 15% [7, 8]. One cannot expect any better agreement from the two methods since they measure different things: ARPES gives us the quasiparticle lifetimes and self-energies for any given k vector whereas the optical self-energy represents an average over the Fermi surface of contributions to the current excited by the external field with each point characterized by a velocity component parallel to the field and a lifetime of this particular quasiparticle. It therefore comes as a surprise that the two methods give very similar results not only for the absolute values of these quantities but also their frequency and temperature dependences, in particular if the ARPES results for quasiparticles near the nodal point are compared with the optical conductivity. Away from the nodes there are large discrepancies: at low temperatures ARPES quasiparticles do not show the narrowing that the optical conductivity shows and there appears to be an inelastic scattering background that is not seen in the optical conductivity.

Many optical studies have been done on the cuprate systems, especially $La_{2-x}Sr_xCuO_4$ (LSCO) and $YBa_2Cu_3O_{6+x}$ (Y123) for light polarized along the ab-plane as well as the less conducting c-axis direction [9]. Much early optical work was done on the important Bi-2212 material [10–13]. Quijada *et al* [12] give a complete set of references to the earliest work. However recent advances in crystal growth with image furnaces have yielded better quality crystals, suggesting a need for new studies of this material. Here we report on the optical properties of the ab-plane of Bi-2212 over a broad doping range from underdoped to overdoped at various temperatures above and below T_c. We obtain various optical quantities

from the measured reflectance and discuss some important doping dependent issues. In particular, we focus on the doping dependent superfluid density and the doping dependence of the contributions of various excitations to the optical self-energy.

The superfluid density is a fundamentally important quantity in superconductivity because it is directly related to the ability of the superconducting wavefunction to resist perturbations to its phase. The superfluid density can be obtained from the optical spectrum in two ways: by analysing the imaginary part of the conductivity as a function of frequency, or by comparing the spectral weight loss in the low frequency region as the superconducting condensate is formed in accord with the Ferrell–Glover–Tinkham (FGT) sum rule [14]. Any discrepancy in the superfluid density obtained by the two methods can be related to the kinetic energy difference between normal and superconducting states. This difference can in turn be related to proposed models of the superconducting mechanism driven by kinetic energy [15–22]. Recent interest has focused on the *doping dependence* of the superfluid density and the kinetic energy difference [16, 19].

The suggestion that spin fluctuations might provide the pairing bosons was made early by the theoretical community [23, 24]. Adding to the interest in magnetic excitations was the absence of an isotope effect in optimally doped samples and the discovery of the sharp magnetic resonance mode at 41 meV in Y123 in the magnetic susceptibility spectrum by inelastic neutron scattering [25–32]. A sharp excitation at this energy can also be seen using other experimental techniques such as optical spectroscopy [8, 33–37], ARPES [38–43], and tunnelling methods [44, 45]. This excitation has the interesting property that its energy $\hbar\Omega$ is proportional to the superconducting transition temperature according to $\hbar\Omega \approx 5\ k_B T$ at all doping levels [31] and in all the cuprate families where large single crystals are available. The only exception are the reduced T_c systems such as LSCO where, while there is a peak in the magnetic susceptibility, a sharp resonance does not develop at low temperature. In the overdoped samples the magnetic resonance appears only below T_c but in underdoped samples it can be seen well above T_c [29, 46]. However even in these systems the resonance grows rapidly in strength at the superconducting transition. This temperature dependence of the mode can also be seen in ARPES spectra in the nodal direction [42, 47]. In view of all these connections to superconductivity it is not surprising that the role of magnetic resonance mode in superconductivity has been discussed widely [29, 48–50].

One possible connection of the magnetic resonance to superconductivity would be through its contribution to the optical and quasiparticle self-energy, where it would have a role similar to the role of phonons in BCS superconductivity [8, 35, 36, 39, 42, 51–53]. The problems with this scenario have been pointed out by several authors. In overdoped Y123 the resonance is not present in the normal state and cannot initiate the transition at T_c. In the highly overdoped state the signature of the resonance vanishes from the optical conductivity at a doping level where T_c is around 60 K [8, 34, 54] in both Bi-2212 and $Tl_2Ba_2CuO_{6+\delta}$ (Tl-2201). A general weakening of the contribution of the magnetic resonance to the carrier self-energy with doping has also been seen in ARPES and tunnelling [42, 45, 47]. It was suggested by Hwang *et al* [8] that the coupling of the resonance disappears above a critical doping level of $p = 0.24$. Other experiments support the idea that there is a significant change in the properties of the cuprates at this doping level. Shibauchi *et al* [55] observed that the pseudogap temperature T^* in c-axis transport merged to T_c in Bi-2212 system near the critical doping, 0.24. Ozyuzer *et al* [56] have observed that there was no indication of a pseudogap near at Fermi level in their tunnelling conductance spectrum of a very overdoped Bi-2212 with $T_c = 56$ K. Some ARPES studies showed that near the critical doping the topology of the Fermi surface transformed from hole-like to electron-like in Pb-doped Bi-2201 [57, 58], LSCO [59] and Bi-2212 [60]. Another ARPES study found that a crossover from two-to

three-dimensional electronic structure occurred near the critical doping with $T_c = 22$ K in $(Bi, Pb)_2(Sr, La)_2CuO_{6+\delta}$ system [61], which has $T_c^{max} = 35$ K.

In addition to the sharp mode there is a continuous bosonic background spectrum that is responsible for the strong linearly rising scattering rate that extends to very high frequencies. It has been discussed in the theoretical literature in the context of models such as the marginal Fermi liquid (MFL) [62] or the interaction of the charge carriers with a continuous spectrum of spin fluctuations with the Millis–Monien–Pines (MMP) spectrum [24]. This broad background exists at all temperatures and doping levels and in all cuprate systems including LSCO system [63], where there is no clear evidence for the presence of the magnetic resonance mode. This ubiquitous feature in the cuprates may be also be responsible for the broad kink feature in ARPES spectra near the nodal region [64]. Other strongly correlated electron systems have similar broad backgrounds in their bosonic spectra or the real part of the optical self-energy—for example, the sodium cobaltate system [65]. Interestingly, the sharp mode and the broad background were captured by optical spectroscopy in the early days for the high temperature superconductors [66].

The rest of the paper is as follows. In section 2 we describe our experimental technique including sample preparation and provide our measured reflectance spectra. In section 3 we describe how we extract the optical conductivity from the measured reflectance and discuss some recent issues on the optical conductivity. In section 4 we extract the superfluid density using two different methods and the kinetic energy change going from the normal to the superconducting state. In section 5 we introduce the optical self-energy using the extended Drude formalism and describe the doping and temperature dependent properties of the self-energy. Finally, in section 6 we relate our experiments to several important recent issues and provide an overall summary of our work.

2. Sample preparation and reflectance

The Bi-2212 single crystals used in the study were grown in an optical image furnace with the travelling solvent floating-zone technique. To get the appropriately doped samples from as-grown crystals we annealed under various oxygen annealing conditions [67]; this yielded good samples of the underdoped (UD), optimally doped (OPT), and overdoped (OD) phases. Unwanted *c*-axis longitudinal phonons can be admixed in *ab*-plane optical data of other cuprates such as LSCO and Y123 [68, 69]. We see no evidence of these in our samples. We were able to obtain shiny optical quality *ab*-plane surfaces Bi-2212 by cleaving the sample.

A commercial Fourier transform spectrometer, Bruker IFS 66v/S, was used to obtain the reflectance data over a wide frequency range from 50 to 40 000 cm^{-1}. For the low temperature measurements we used a continuous flow liquid helium cryostat with an automated temperature control and sample change system [70] to improve the reproducibility over a manual system. A polished stainless steel mirror was used as an intermediate reference to correct for the instrument drift with time and temperature. An *in situ* evaporated gold (50–14 000 cm^{-1}) or aluminium (12 000–40 000 cm^{-1}) film on the sample was used as the final reflectance reference [71]. The reflectance of the gold films was in turn calibrated with a polished stainless steel sample where we relied on the Drude theory and the dc resistivity as the ultimate reference. An advantage of this method is that it corrects for geometrical effects of an irregular surface. The *in situ* gold evaporation technique gives accurate temperature dependent data with an accuracy better than $\pm 0.05\%$ at room temperature.

We measured reflectance of four overdoped ($T_c = 80$, 82, 65, and 60 K), one optimally doped ($T_c = 96$ K), and one underdoped ($T_c = 69$ K) Bi-2212 sample. We estimated the

Table 1. Doping levels (p), the background dielectric constant (ϵ_H), and the plasma frequency (ω_p) of our eight Bi-2212 samples. $\gamma(p)$ is obtained from the power law in the optical conductivity (see section 3.2).

Samples	T_c (K)	Doping level, p	ϵ_H	ω_p (cm^{-1})	$\gamma(p)$
UD67	67	0.103	4.27	15 050	1.527
UD69	69	0.106	5.51	16 560	1.563
UD82	82	0.125	4.42	16 300	1.454
OPT96	96	0.160	4.77	17 000	1.449
OD82	82	0.195	5.45	18 800	1.378
OD80	80	0.198	5.07	18 310	1.335
OD65	65	0.219	5.58	19 200	1.332
OD60	60	0.224	5.52	18 900	1.333

hole doping levels of the samples using the empirical parabolic equation of Presland *et al* [72]: $p(T_c) = 0.16 \mp [1/82.6\,(1 - T_c/T_c^{max})]^{1/2}$, where T_c^{max} is the maximum T_c of the material. The determination of T_c^{max} is not an easy problem [67] as it depends on the growth conditions and dopant levels. In the absence of a better method, we use the generally accepted value of 91 K as the T_c^{max} for Bi-2212. We should mention here that our optimally doped sample is doped with a small amount of Y to yield a relatively well ordered system and shows a surprisingly high $T_c = 96$ K [67] and we assigned $p = 0.16$ as its hole doping level. The disadvantage of the parabolic approximation is that it does not uniquely determine the doping level of the sample since there are two independent p values for each value of T_c. To avoid the ambiguity in the determination of the doping levels we used the slope of the infrared reflectance as an additional test of the doping level [73]. Table 1 shows the estimated doping levels of our eight Bi-2212 samples.

Figure 1 displays the measured ab-plane reflectance of Bi-2212 at eight different doping levels and at various temperatures. As the hole doping level increases, some interesting doping dependent features show up; the overall reflectance level increases and the overall shape becomes more curved. For each doping level, as the temperature decreases the overall reflectance increases because of the reduced scattering and, more interestingly, a shoulder appears between 500 and 1000 cm^{-1} below an onset temperature, which is also doping dependent. We will analyse the shoulder feature in detail and discuss its doping dependent properties in section 5. At room temperature the reflectance below 2000 cm^{-1} is approximately linear in frequency. This linear variation, the so-called marginal Fermi liquid behaviour [62] in Bi-2212 at 300 K has been analysed in detail by Hwang *et al* [73] below 2000 cm^{-1} over a wide doping range.

3. Optical conductivity

In this section we provide the optical conductivity derived from the reflectance by using Kramers–Kronig (KK) transformations [12, 74–76]. To use this method we have to extrapolate the measured reflectance to zero frequency on the low frequency side of the measured range and to infinite frequency on the high frequency side. We used the following extrapolations. For $\omega \to 0$, the reflectance was extrapolated by assuming a Hagen–Rubens frequency dependence, $1 - R(\omega) \propto \omega^{1/2}$ for normal states and $1 - R(\omega) \propto \omega^4$ for the superconducting states. For $\omega \to \infty$, the reflectance has been extended by using literature data [77] and free electron behaviour ($R \propto \omega^{-4}$).

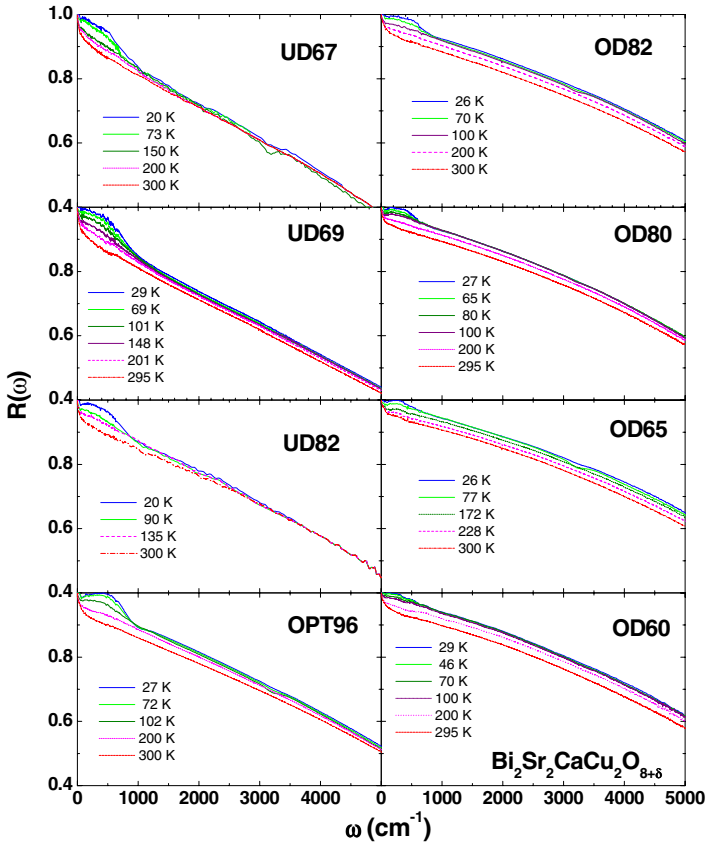

Figure 1. *ab*-plane reflectance of Bi-2212 at eight different doping levels. The overall reflectance increases as the hole doping level increases with charge carrier density introduced by doping. Here and in the following figures we use a shorthand notation to describe doping status of our samples; for example UD67 stands for the underdoped sample with $T_c = 67$ K, OD for overdoped and OP for optimal doping. We note that a dip feature near 3300 cm^{-1} of the low temperature data of some of the samples an absorption is a band from ice on the sample. This feature does not affect low frequency data below the absorption frequency, 3300 cm^{-1}. However it affects the high frequency data above 3300 cm^{-1}.

To obtain further optical constants from the measured reflectance ($R(\omega)$) and the corresponding calculated phase ($\phi(\omega)$) from KK analysis, we used Fresnel's equation for normal incidence as an approximation:

$$\frac{1 - n(\omega) - \mathrm{i}k(\omega)}{1 + n(\omega) + \mathrm{i}k(\omega)} = \sqrt{R(\omega)}\mathrm{e}^{\mathrm{i}\phi(\omega)} \tag{1}$$

or

$$n(\omega) = \frac{1 - R(\omega)}{1 + R(\omega) - 2\sqrt{R(\omega)}\cos\phi(\omega)} \tag{2}$$

$$k(\omega) = \frac{-2\sqrt{R(\omega)}\sin\phi(\omega)}{1 + R(\omega) - 2\sqrt{R(\omega)}\cos\phi(\omega)} \tag{3}$$

where $n(\omega)$ and $k(\omega)$ are the index of refraction and the extinction coefficient, respectively.

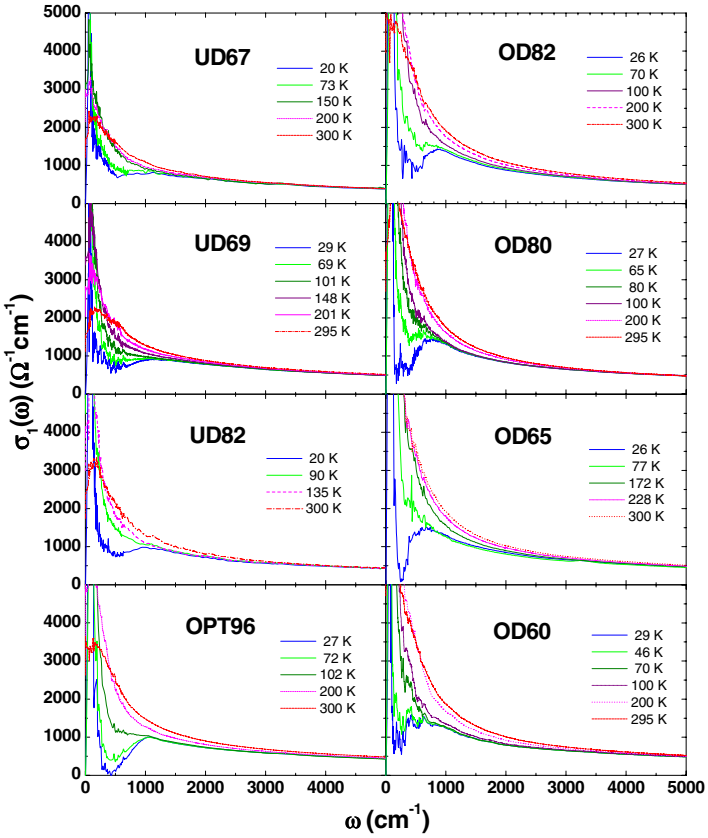

Figure 2. The *ab*-plane optical conductivity of Bi-2212 of eight Bi-2212 samples at various temperatures above and below T_c.

In principle, we are able to obtain any other optical quantities by using the various relationships between the optical quantities [74]:

$$\epsilon_1(\omega) = n^2(\omega) - k^2(\omega) \tag{4}$$

$$\epsilon_2(\omega) = 2n(\omega)k(\omega) \tag{5}$$

and

$$\sigma(\omega) = -\mathrm{i}\frac{\omega}{4\pi}[(\epsilon_1(\omega) - \epsilon_\mathrm{H}) + \mathrm{i}\epsilon_2(\omega)] \tag{6}$$

where $\epsilon_1(\omega)$ and $\epsilon_2(\omega)$ are the real and imaginary parts of the optical dielectric constant, respectively, and $\sigma(\omega) \equiv \sigma_1(\omega) + \mathrm{i}\sigma_2(\omega)$ is the complex optical conductivity.

Figure 2 displays the real part of the optical conductivity of Bi-2212. We observe strong temperature dependence only in the low frequency region, below 3000 cm^{-1}. The spectral weight or the number of effective charge carriers per Cu atom on CuO_2 plane is defined as follows:

$$N_\mathrm{eff}(\omega_c) = \frac{2mV_\mathrm{Cu}}{\pi e^2}\int_{0^+}^{\omega_c} \sigma_1(\omega')\,\mathrm{d}\omega' \tag{7}$$

where ω_c is the cut-off frequency, m is the free electron mass, V_Cu is the volume per Cu atom in the sample, e is the charge of an electron, and σ_1 is the real part of the optical

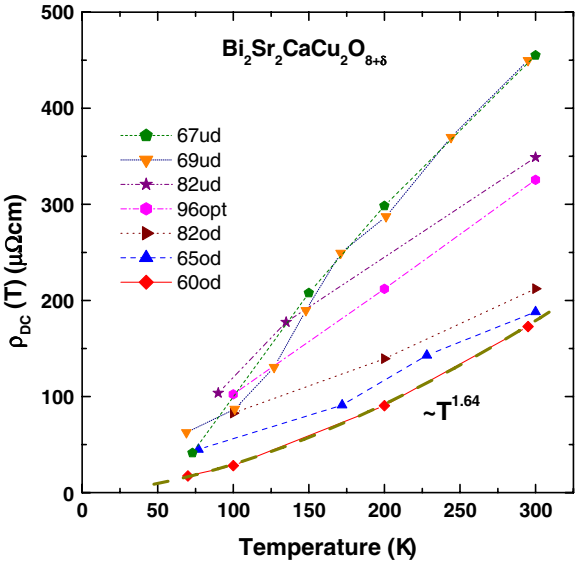

Figure 3. The dc resistivity, $\rho_{\rm dc}(T)$, extracted from low frequency extrapolations of normal state optical conductivities. The dashed curve through the data points for our most overdoped sample is a fitted curve, $\rho_{\rm dc}(T) = 0.0155\ T^{1.64}$. See the text for a detailed description of the extrapolation.

conductivity. The spectral weight is proportional to the area under the $\sigma_1(\omega)$ curve. As the hole doping increases the overall conductivity increases. For each doping level, as the temperature decreases, the spectral weight at low frequencies increases as a result of the narrowing the Drude-like absorption band near zero frequency. This shift of spectral weight continues down to the superconducting transition temperature, $T_{\rm c}$. Below or near $T_{\rm c}$ a strong depression of spectral weight below 1000 cm^{-1} sets in and grows with decreasing temperature. This feature is related to the step-like feature in the optical scattering rate. (For more detailed discussion see section 5.) The missing area between the normal and the superconducting curves can be a measure of the superfluid density (for more detailed discussion see section 4). Even in the superconducting state we have a sizable amount of residual spectral weight near zero frequency, which is absent in the conventional superconductors [78–81].

In figure 3 we show the temperature dependence of the dc resistivity of our eight Bi-2212 samples obtained from extrapolations to zero frequency of the normal state optical conductivities. These optically determined resistivities show the same features and trends as are seen with four-probe dc measurements. Starting with the optimally doped sample OPT96 we see the familiar linear variation of resistivity with temperature with a zero-temperature intercept that is very close to the zero of the temperature axis. From the beginning of the study of the cuprates this behaviour has been taken as evidence of an exotic transport mechanism. Interaction with a bosonic mode would also be linear with temperature in this range but would yield an intercept at approximately $\hbar\omega/4$ where ω is the frequency of the mode. For phonon modes involving oxygens this intercept would be at 100 K. Moving to underdoped samples we do find a higher intercept associated with the temperature dependence below about 150 K. Above this temperature the temperature dependence is similar to that of the optimally doped sample with a lower intercept on the temperature axis. The overdoped samples on the other hand show a more metallic temperature dependence with an upward curvature with the power law index of 1.64 for our most overdoped sample, smaller than the T^2 expected for a Fermi

liquid. These observations are consistent all previous systematic measurements of the dc resistivity [82, 83]. The message from the underdoped samples is that any bosonic spectral function causing this scattering has a temperature dependent amplitude with rapid changes occurring in the 150 K temperature range. This is in agreement with our study of another underdoped system, orthoII YBCO [53].

3.1. ϵ_H and σ_2

The quantity ϵ_H is the contribution to the dielectric constant from all the high frequency spectral weight but excluding the low frequency free carrier or intraband contribution. It is often difficult to determine where the dividing line between the free carriers and the interband absorption lies. Here we explain the method which we use to estimate ϵ_H. First of all we assume that the frequency which divides the free charge carrier band and the charge transfer interband absorption is known. We call this characteristic frequency the separating frequency, ω_{sp}. For a given separating frequency we can determine both the plasma frequency, ω_p, and the dielectric constant at high frequency, ϵ_H as follows. The ω_p can be estimated using the following equation:

$$\omega_p = \sqrt{\frac{120}{\pi}\int_0^{\omega_{sp}} \sigma_1(\omega')\,d\omega'} \tag{8}$$

where all frequencies are in cm^{-1}. The magnitude of ϵ_H can be determined from a Kramers–Kronig transformation of the high frequency part of σ_1, above ω_{sp}:

$$\epsilon_H \equiv \epsilon_1(\omega)|_{\omega\to 0} = 1 + \frac{120}{\pi} P \int_{\omega_{sp}}^{\infty} \frac{\sigma_1(\omega')}{\omega'^2 - \omega^2}\,d\omega' \tag{9}$$

where P denotes the Cauchy principal value, frequencies are in cm^{-1}, and σ_1 in Ω^{-1} cm^{-1}. In figure 4 we show an example of an application of the method for optimally doped Bi-2212 at $T = 102$ K with a given $\omega_{sp} = 21\,000$ cm^{-1}. Here we estimate $\omega_p = 19\,450$ cm^{-1} and $\epsilon_H = 4.34$.

To estimate ϵ_H first get the separating frequency ω_{sp} using the method which we introduced in a previous paper [73] where we extrapolate the absorption coefficient α of the free carrier absorption to zero frequency. Then we use equation (8) to obtain the plasma frequency ω_p and equation (9) to obtain ϵ_H. We show the dependence of ω_p and ϵ_H on the separating frequency in figure 5. While there is a large variation in plasma frequency there is only a small variation in ϵ_H for ω_{sp} values between the well separated bands: the free charge carrier band (below 10 000 cm^{-1}) and the charge transfer band (above 30 000 cm^{-1}). Our estimated ϵ_H and ω_p for our eight different Bi-2212 samples are shown in table 1. We used data at $T = 300$ K, which are the most accurately measured with our experimental technique. One thing we should mention here is that we do not have accurate high frequency data above 6 eV for all doping levels. To get σ_2 we used ϵ_H values in table 1 (see equation (6)). Recently, the accuracy of the various methods of finding ϵ_H has become an important issue because the optical scattering rate is very sensitive to the value of ϵ_H, especially at high frequency (for more discussions see the following section 3.2 and figure 9 and the related text).

3.2. Optical conductivity: amplitude and phase

The complex optical conductivity can be described by an amplitude and a phase, i.e. $\sigma(\omega) = |\sigma(\omega)|e^{i\Phi(\omega)}$, where $|\sigma(\omega)| = \sqrt{\sigma_1^2(\omega) + \sigma_2^2(\omega)}$, and $\Phi(\omega) = \tan^{-1}(\sigma_2(\omega)/\sigma_1(\omega))$. Anderson [84] suggested a simple power law behaviour for the complex optical conductivity in

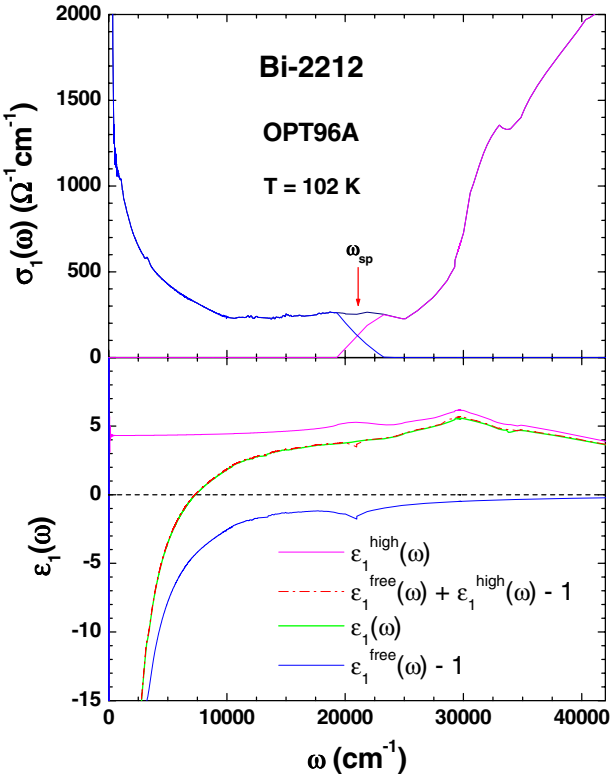

Figure 4. Separate contributions to ϵ_1 of free charge carriers and high frequency bands divided by a separating frequency, $\omega_{sp} = 21\,000\ \mathrm{cm}^{-1}$.

his Luttinger liquid model. Recently van der Marel *et al* [85] revisited the Anderson's model, describing the optical conductivity as $\sigma(\omega) = C(-\mathrm{i}\omega)^{\gamma-2}$, where C is a frequency independent constant. In this description we have $|\sigma(\omega)| = C\omega^{\gamma-2}$ and $\Phi(\omega) = \pi/2(2-\gamma)$, which is frequency independent. In figure 6 we plot the amplitude of the optical conductivity for our eight Bi-2212 samples at various temperatures on a log–log scale. The dashed lines are linear least squares fits of the amplitude between 500 and 5000 cm^{-1} in the normal state where the quantity $|\sigma(\omega)|$ shows negligible temperature dependence. The absolute value of the slope $(\gamma - 2)$ of the fitted straight line increases as the doping level increases. From the slope we can obtain the doping dependence of $\gamma(p)$ shown in table 1, which decreases monotonically from 1.55 to 1.33 as doping increases (see figure 8).

In figure 7 we show the phase, $\Phi(\omega)$, of the optical conductivity for all our samples. We note that the phase is almost frequency independent over a wide spectral range above 1000 cm^{-1} at all measured temperatures. The dashed horizontal line is the corresponding phase of the straight line fit of the amplitude (see figure 6). We observe that the power law behaviour holds over a wide spectral range, roughly between 500 cm^{-1} and near 5000 cm^{-1}, at various temperatures, and over a wide rage of doping. We also note that at low frequencies, below 500 cm^{-1}, the optical conductivity shows a strong temperature dependence and deviates markedly from a constant. In figure 8 we plot the doping dependent exponent, $\gamma(p)$, which is extracted from the linear fits in figure 6. The exponent decreases monotonically as the doping increases. The dot–dashed line is a least squares fit of a straight line to the data. The

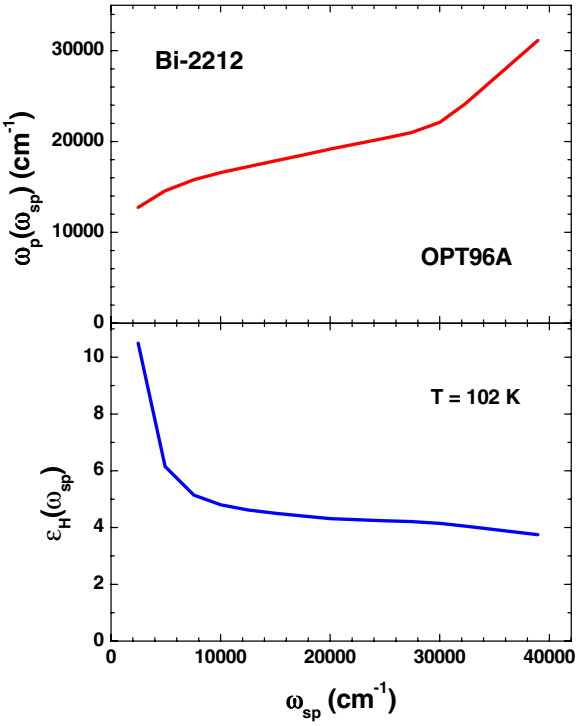

Figure 5. Separating frequency dependence of the plasma frequency (ω_p) and of the high frequency dielectric constant (ϵ_H).

lower dashed line is a predicted variation of this quantity with doping from a recent paper by Anderson [86].

In figure 9 we demonstrate how the value ϵ_H affects the amplitude and the phase of the optical conductivity. Note that ϵ_H affects only the imaginary part of the optical conductivity, σ_2. To see the effect we choose the data for optimally doped Bi-2212 at $T = 102$ K and calculate the complex optical conductivity for four different values of ϵ_H between 2.50 and 6.00. It is clear from the figure that there is no significant effect below 1000 cm^{-1} but the effect builds up rapidly as the frequency increases. In the upper panel we show calculated amplitudes on a log–log scale. As ϵ_H increases, the absolute value of the slope in the amplitude between 500 and 5000 cm^{-1} decreases. In the lower panel we show corresponding phases. As ϵ_H increases, the slope in the phase changes from negative to positive. We introduced and described a useful method for estimating ϵ_H in section 3.1.

4. FGT sum rule, superfluid density and kinetic energy

There are various techniques used to determine the superfluid density including optics. Optics has the advantage that it gives the absolute value and in an anisotropic system (such as the high temperature cuprates), it also provides all the orthogonal components if a well oriented crystal is used. However, there are problems that make an accurate determination of the absolute magnitude difficult. The first of these is a need to determine accurately the reflectance in the low frequency region where the it approaches unity and where measurements on small crystals are difficult as the wavelength of the radiation used approaches the size of the samples.

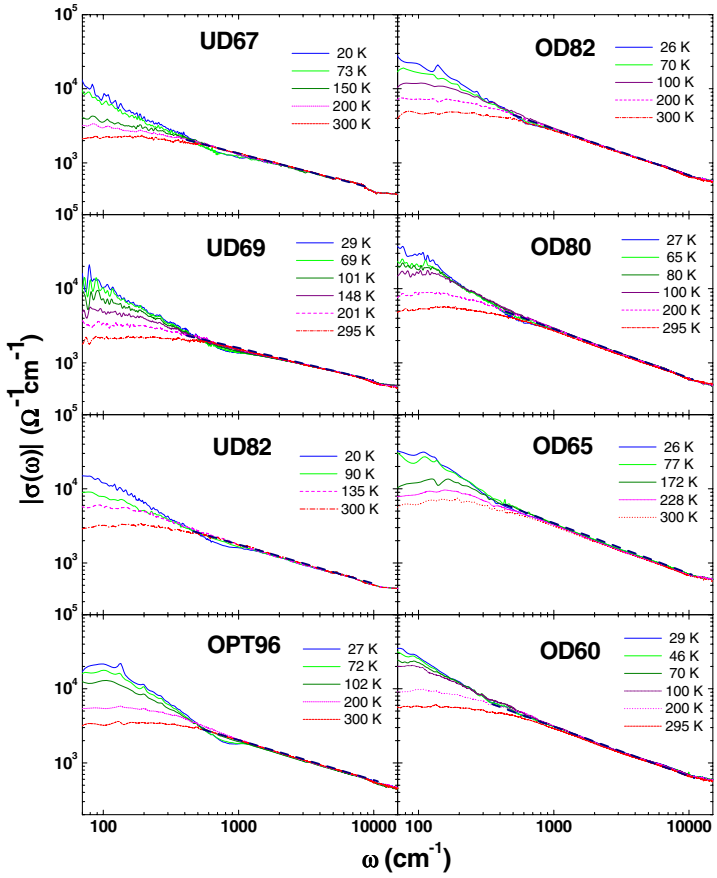

Figure 6. Amplitude of the optical conductivity, $|\sigma(\omega)| \equiv \sqrt{\sigma_1^2(\omega) + \sigma_2^2(\omega)}$. The dashed lines are least squares fits of the temperature independent region.

Another source of uncertainty is the presence of a residual metallic conductivity in the superconducting state seen in many samples. This effect can be recognized from a downturn in reflectance at low frequency by as much as one to two per cent. The resulting conductivity shows a peak removed from zero frequency, characteristic of a disordered metallic material [87]. This low frequency suppression of reflectance is directly related to a sizable low frequency spectral weight in the optical conductivity and might cause some uncertainty in the estimated superfluid density. Here we try to minimize this uncertainty by estimating the superfluid density with the same criteria for all our Bi-2212 samples using the same experimental instrument and technique, the same method of analysis, and the same low frequency cut-off of reflectance data, 50 cm^{-1}. With eight different data sets for the optical conductivity of Bi-2212, we obtain doping dependent superfluid density from the highly underdoped region to the overdoped region.

Figure 10 shows the frequency dependent accumulated spectral weight or the effective number of charge carriers per Cu atom of eight Bi-2212 samples at various temperatures below and above T_c. Overall, the spectral weight increases as we add carriers by doping as we expect. In the normal state, as the doping level increases, the temperature dependent region in the

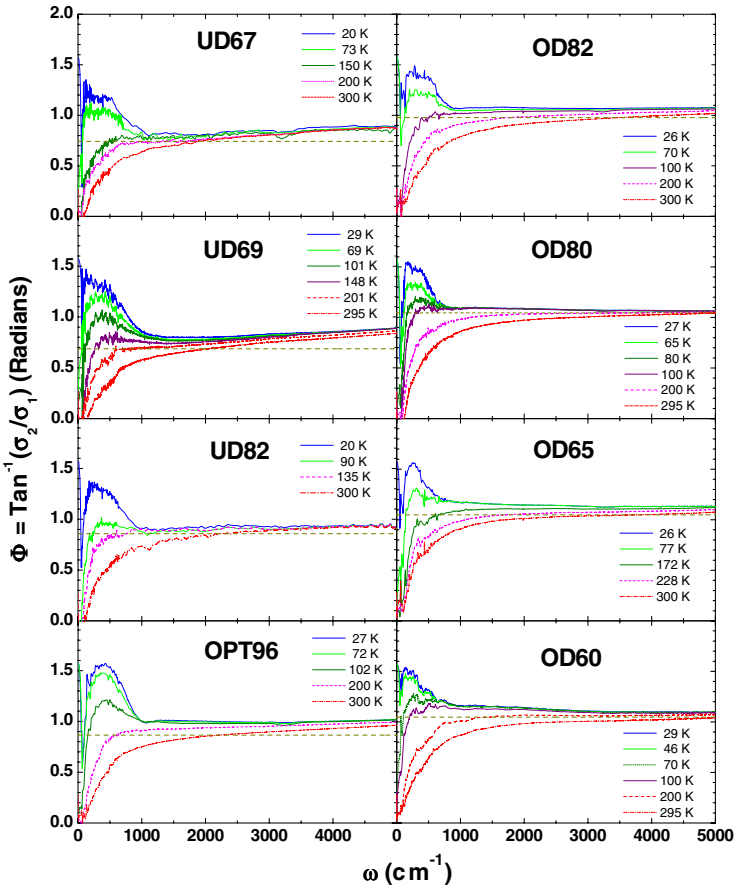

Figure 7. Phase of the optical conductivity, $\Phi(\omega) \equiv \tan^{-1}(\sigma_2(\omega)/\sigma_1(\omega))$ [85]. The dashed horizontal lines are obtained from the fitted straight lines in figure 6.

spectral weight extends to higher frequency. As the temperature is lowered, spectral weight is shifted to low frequency because of the narrowing of the Drude band.

Above 2000 cm^{-1} the highest spectral weight curves are almost parallel to the curve in the superconducting state. The difference between the two parallel spectral weight curves gives us a rough estimate of the number of superfluid charge carriers per Cu atom, the superfluid density. This difference increases as the doping level increases; the higher the doping level, the higher the superfluid density (see figure 14). The flat region spectral weight in the superconducting state is related to the dip below 1000 cm^{-1} in the optical conductivity. We analyse spectral weight variations in detail using the optical sum rule [74, 79] with and without including the temperature dependence in the spectral weight.

4.1. Temperature and doping dependence of the optical spectral weight at the normal state

The temperature dependence of the optical spectral weight has been studied by several experimental groups [17, 19, 21, 88, 89]. Those groups have found a quadratic temperature dependence of the spectral weight. There are many theoretical studies on temperature dependent optical spectral weight [15, 16]. The spectral weight as a function of temperature

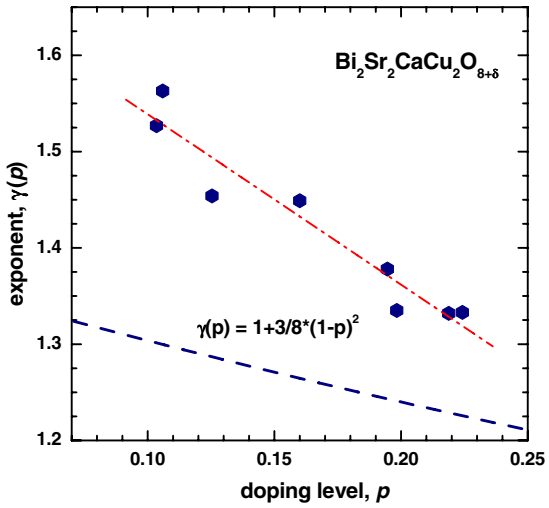

Figure 8. Doping dependent exponent, $\gamma(p)$. See the text for a detailed description of the quantity $\gamma(p)$. The dashed line is a theoretical estimate of the variation of $\gamma(p)$ with doping due to Anderson [86].

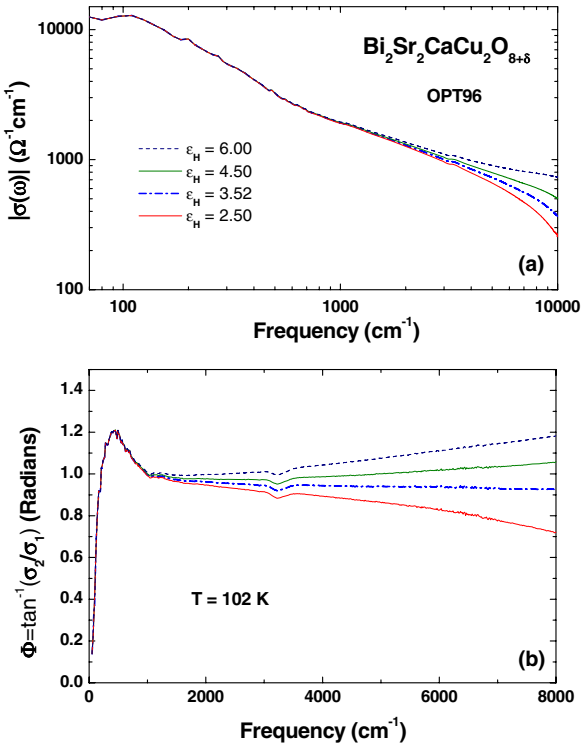

Figure 9. The effect of choosing different values of ϵ_{H} on the amplitude (a) and the phase (b) of the optical conductivity. Note that σ_1 is independent of ϵ_{H}.

consists of two terms, one going like T and the other like T^2; the T linear term is attributed to strong correlations among the carriers and the T^2 term is attributed to the thermally excited

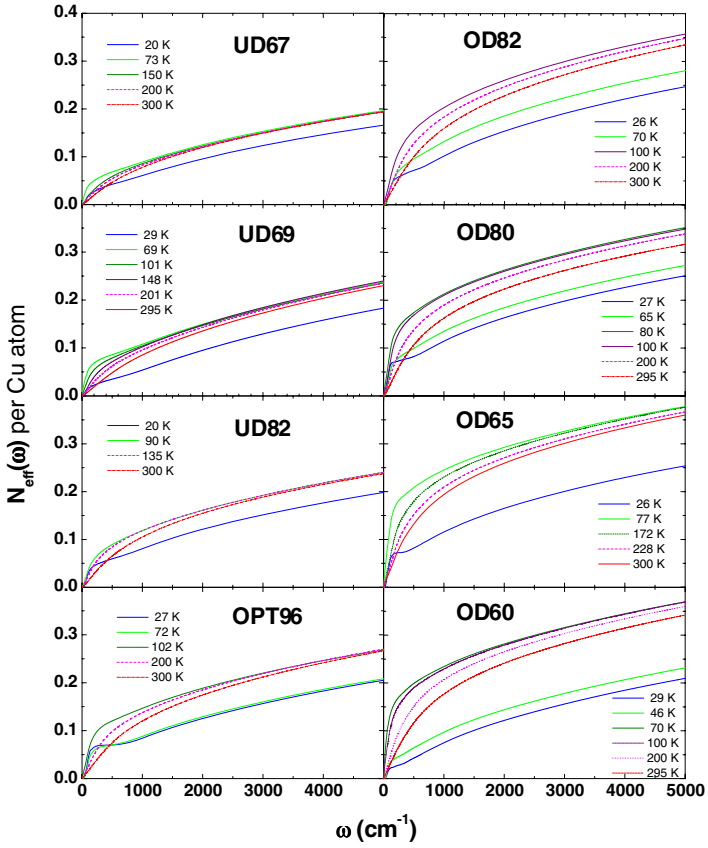

Figure 10. Frequency dependent spectral weight expressed as the number of effective charge carriers per Cu atom of Bi-2212, as defined in equation (7).

free carrier contribution [88]. The large prefactor of the T^2 term can carry information on correlations [89]. In figure 11 we show the temperature dependent spectral weight normalized to the lowest normal temperature (T_L), $N_{eff}(T)/N_{eff}(T_L)$, for three representative samples of UD69, OD80, and OD60 for several different cut-off frequencies (see equation (7) and [89]): 500, 1000, 5000, and 10 000 cm^{-1}. The overall trend is that the spectral weight decreases as temperature increases. The left (right) panels display the normalized spectral weight as a function of T (T^2). We are able to clearly find a cut-off frequency and the doping dependence of the spectral weight in the figure. For the four different cut-off frequencies a linear in T law alone gives better agreement with data than a T^2 term alone. For the lowest cut-off frequency (500 cm^{-1}) the linear term is more dominant; T linear holds well for the two overdoped samples and T sublinear holds better for the underdoped sample. For a higher cut-off (5000 cm^{-1} or higher) the quadratic term is dominant; T^2 works well for all dopings. Our observation agrees with that of Bontemps *et al* [90].

In figure 12 we display the temperature dependent $N_{eff}(T)$ for our six representative Bi-2212 samples with a cut-off frequency of 2000 cm^{-1}. Above T_c as the temperature decreases N_{eff} increases almost linearly and the rate of increase grows as the doping level increases. We take into account this approximated linear temperature dependence of N_{eff} when we adjust the superfluid density, $N_{s,sum}$ (see figure 15), to obtain the kinetic energy change.

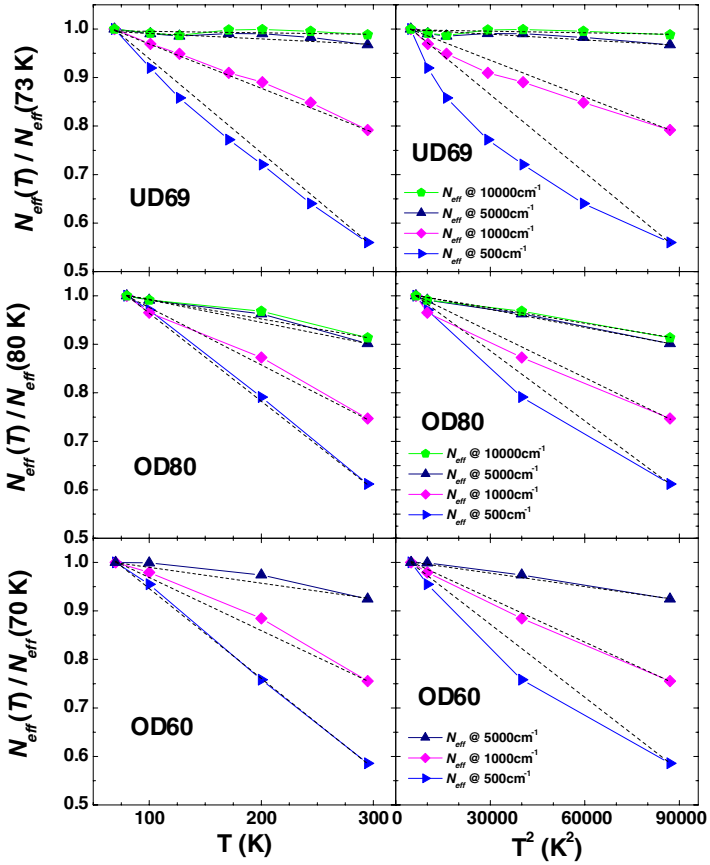

Figure 11. Doping and cut-off frequency dependent temperature dependence of the spectral weight for three representative Bi-2212 samples: UD69, OD80, and OD60, plotted as a function of T, left panels, and T^2, right panels.

4.2. Superfluid density from the optical conductivity

We describe next the method we use to obtain the superfluid density from the optical conductivity in the superconducting state [91]. In the superconducting state we have two separate contributions to the real part of the optical conductivity: a delta function at the origin from the superconducting condensate and a regular non-superconducting part

$$\sigma_1(\omega) = \sigma_{1s}\delta(0) + \sigma_1'(\omega) \tag{10}$$

where σ_{1s} is a contribution from the superfluid charge carriers and $\sigma_1'(\omega)$ is a regular non-superconducting part of the optical conductivity. From the optical sum rule, we can describe the superfluid plasma frequency, ω_{ps}, in terms of σ_{1s}; $\sigma_{1s} = \omega_{ps}^2/8 = \pi n_s e^2/(2m)$, where n_s is the superfluid density and m is the mass of an electron. Note that the dimension of σ_{1s} is frequency squared. The Kramers–Kronig (KK) transformation of the real part gives us the imaginary part, which also consists of two terms, as follows:

$$\sigma_2(\omega) \equiv \sigma_{2s}(\omega) + \sigma_2'(\omega) \tag{11}$$

$$= \frac{2\sigma_{1s}}{\pi\omega} + \sigma_2'(\omega) \tag{12}$$

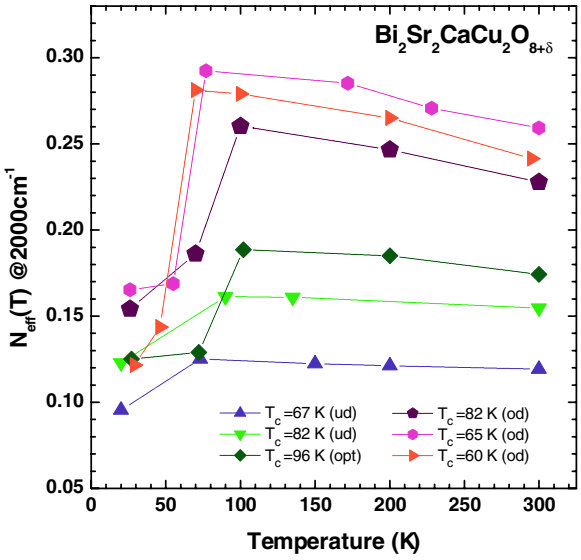

Figure 12. Temperature dependent spectral weight below 2000 cm^{-1} for six representative Bi-2212 samples. At this cut-off frequency the spectral weight increases as the temperature is lowered to drop rapidly at T_c as the superconducting condensate forms. There is a monotonic increase of spectral weight with doping.

where $\sigma_{2s}(\omega)$ is the imaginary part of the condensate conductivity and $\sigma_2'(\omega)$ the imaginary part of the regular non-superconducting part. The latter makes a KK pair with $\sigma_1'(\omega)$.

Here we explain how we get the σ_{2s} from the optical conductivity. Using another KK transformation we can calculate σ_2' from σ_1', which is simply the regular non-superconducting optical conductivity in the superconducting state because σ_{1s} is a delta function at zero frequency, which is excluded in the KK and is not seen at finite frequencies. We have already extracted the total σ_2 from the measured reflectance and a given ϵ_H by using KK analysis as described previously (see section 3). So we can obtain σ_{2s} by subtracting σ_2' from σ_2 (see equation (3)). Finally, we can calculate the superfluid plasma frequency, which is closely related to the superfluid density per copper, N_s, by the following equation:

$$\sigma_{2s}(\omega)\cdot\omega = \frac{2\sigma_{1s}}{\pi} = \frac{\omega_{ps}^2}{4\pi} = \frac{N_s e^2}{m V_{Cu}} \tag{13}$$

where V_{Cu} is the volume per Cu atom, e is the charge of an electron, and m is the mass of a free electron.

After some unit conversions, we get the following practical formula for the superfluid density, N_s:

$$N_s \cong 6.29\times 10^{-10} V_{Cu}\cdot\sigma_{2s}(\omega)\cdot\omega \tag{14}$$

where V_{Cu} is in $Å^3$, σ_{2s} in Ω^{-1} cm^{-1}, and ω in cm^{-1}. For Bi-2212 V_{Cu} is 112.6 $Å^3$, which does not change much with doping.

Another independent method that yields the superfluid density from the optical conductivity is directly related to the 'missing spectral weight' in the optical conductivity when charge carriers are paired and condense to form the superfluid. There is a fundamental difference between this and the previous method. For this method we need to have two optical conductivities (one in the normal state and the other in the superconducting state) but only

one optical conductivity in the superconducting state is needed for the application of the previous method. We should note that the temperatures of the normal and superconducting states are not the same. The temperature difference may cause an unwanted error in the superfluid density extracted using this method because the normal state spectral weight shows a temperature dependence (see figure 12) [53, 89] which will extend below the superfluid transition temperature. This method originates in the Ferrel–Glover–Tinkham (FGT) sum rule [14] which states that all the spectral weight lost at finite frequencies is transferred to the superconducting condensate delta function at zero frequency. In the formalism we can describe the superfluid plasma frequency in convenient units as follows:

$$\begin{aligned} \omega^2_{\mathrm{ps,sum}}(\omega) &= \frac{120}{\pi}\int_{0^+}^{\omega}[\sigma_{1,\mathrm{n}}(\omega') - \sigma_{1,\mathrm{s}}(\omega')]\,\mathrm{d}\omega' \\ N_{\mathrm{s,sum}}(\omega) &\cong 4.26\times 10^{-10}\cdot V_{\mathrm{Cu}}\int_{0}^{\omega}(\sigma_{1,\mathrm{n}} - \sigma_{1,\mathrm{s}})\,\mathrm{d}\omega' \end{aligned} \tag{15}$$

where $\sigma_{1,\mathrm{n}}$ and $\sigma_{1,\mathrm{s}}$ are the real parts of the optical conductivity for normal and superconducting states, respectively. V_{Cu} is in $\mathrm{\AA}^3$ and the σ_1 s are in Ω^{-1} cm^{-1}. All frequencies are in cm^{-1} including $\omega_{\mathrm{ps,sum}}$.

In conventional superconductors, where the pairing and the condensation are driven by potential energy, the FGT sum rule holds exactly. However, as Hirsch has proposed, the FGT sum rule can be violated in unconventional superconductors including the cuprates [15] and a modified FGT sum rule can be introduced with an extra kinetic energy terms as follows [16, 92]:

$$\omega^2_{\mathrm{ps}}(\omega) = \frac{120}{\pi}\int_{0^+}^{\omega}\Delta\sigma_1(\omega')\,\mathrm{d}\omega' + \frac{e^2ab}{\pi\hbar^2c^2V_{\mathrm{Cu}}}\Delta E_{\mathrm{Kin}}(\omega)$$

or

$$\Delta E_{\mathrm{Kin}}(\omega) = \frac{\hbar^2}{mab}[N_{\mathrm{s}} - N_{\mathrm{s,sum}}(\omega)] \tag{16}$$

or

$$\Delta E_{\mathrm{Kin}}(\omega) \cong 0.261\times[N_{\mathrm{s}} - N_{\mathrm{s,sum}}(\omega)]\ (\mathrm{in\ eV}) \tag{17}$$

where $\Delta\sigma_1(\omega') = \sigma_{1,\mathrm{n}}(\omega') - \sigma_{1,\mathrm{s}}(\omega')$, a and b are the lattice constants of the ab-plane, c is the speed of light, and $\Delta E_{\mathrm{Kin}}(\omega)$ is the kinetic energy change when the system becomes a superconductor, i.e. $\Delta E_{\mathrm{Kin}}(\omega) \equiv E^{\mathrm{s}}_{\mathrm{Kin}}(\omega) - E^{\mathrm{n}}_{\mathrm{Kin}}(\omega)$, where $E^{\mathrm{s}}_{\mathrm{Kin}}(\omega)$ and $E^{\mathrm{n}}_{\mathrm{Kin}}(\omega)$ are the kinetic energies of the superconducting and the normal states, respectively. Note that equation (17) holds only for Bi-2212 systems. In figure 13 we show the superfluid densities obtained from the two different methods, i.e. using equations (14) and (15). Here we do not include the temperature dependence of N_{eff} to obtain $N_{\mathrm{s,sum}}(\omega)$ yet. In principle, $N_{\mathrm{s}}(\omega)$ is frequency independent and $N_{\mathrm{s,sum}}(\omega)$ approaches a saturation value as the frequency increases. We observe that $N_{\mathrm{s,sum}}$ saturates more quickly as doping increases, which is consistent with the observation of Homes *et al* [93] in the $YBa_2Cu_3O_{6+x}$ (Y123) system, except that our saturation frequency is lower than what they observed. The number in the parentheses is a percentage difference between N_{s} and the saturated $N_{\mathrm{s,sum}}$, i.e. $(N_{\mathrm{s}} - N_{\mathrm{s,sum}})/N_{\mathrm{s}} \times 100$. Roughly, we observe that the superfluid density increases as doping increases. Through the whole spectral range and at all doping levels the saturated $N_{\mathrm{s,sum}}$ is smaller than N_{s} and the FGT sum rule is violated. However, when we take into account the temperature dependence for $N_{\mathrm{s,sum}}$, $N_{\mathrm{s,sum}}$ is smaller than N_{s} in the underdoped region and is larger than N_{s} in the overdoped region (see figure 15). In other words the sum rule violation changes sign at this doping level.

In the upper panel of figure 14 we show a T_{c} versus $\rho_{\mathrm{s}} \equiv \omega^2_{\mathrm{ps}}$ graph. We do not observe the so-called 'boomerang' effect [94, 95] where at higher doping levels the superfluid density

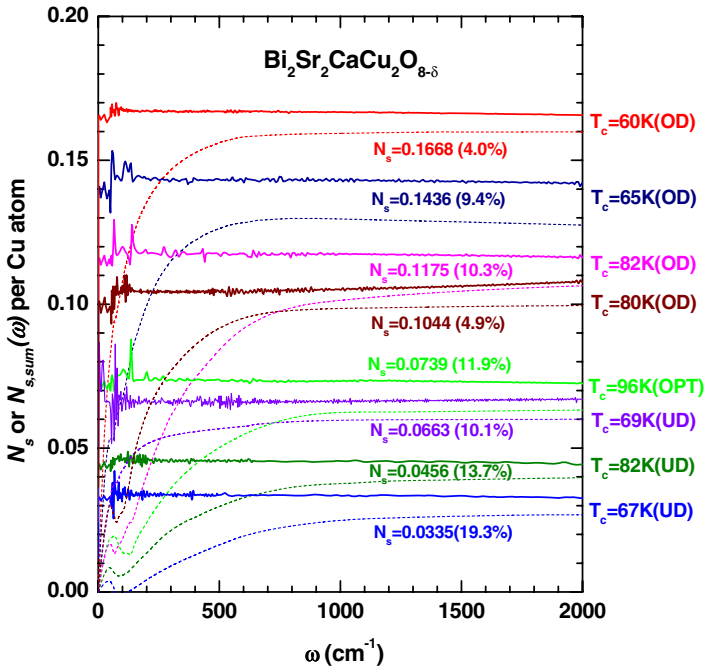

Figure 13. Superfluid densities obtained by two different methods using $\sigma_2(\omega)$ (equation (14)) (solid curves) and using the FGT sum rule (equation (15)) (dashed curves). See table 2 for detailed values of N_s.

Table 2. Superfluid densities of our eight Bi-2212 samples. N_s are the superfluid densities extracted using equation (14) and $N_{s,sum}$ are the superfluid densities extracted using the FGT sum rule, equation (15), integrated up to 2000 cm^{-1}. $N_{s,diff}$ (%) are the percentage differences between superfluid densities determined by the two methods (see the text for a more detailed description).

Samples	T_c (K)	p	N_s	$N_{s,sum}$	$N_{s,diff}$ (%)
UD67	67	0.103	0.0335	0.0270	19.3
UD69	69	0.106	0.0663	0.0596	10.1
UD82	82	0.125	0.0456	0.0394	13.7
OPT96	96	0.160	0.0739	0.0651	11.9
OD82	82	0.195	0.1175	0.1054	10.3
OD80	80	0.198	0.1044	0.0993	4.9
OD65	65	0.219	0.1436	0.1301	9.4
OD60	60	0.224	0.1668	0.1601	4.0

decreases. Also we add two additional data points for 6% Sr-doped LSCO ($T_c = 5.5$ K) and a well ordered underdoped orthoII Y123 ($T_c = 59$ K) [53]. In the lower panel we show the doping dependent London penetration depth, $\lambda_L(p) \equiv 1/(2\pi\omega_{ps})$, where ω_{ps} is in units of cm^{-1}. As doping increases the London penetration depth decreases monotonically with values ranging between 1000 and 3000 Å.

In figure 15 we show the doping dependent kinetic energy change, $\Delta E_{Kin}(p)$, of Bi-2212 samples with two different cut-off frequencies: 1000 and 2000 cm^{-1}. When calculating $\Delta E_{Kin}(p)$ we take into account the temperature dependent spectral weight (see figure 12) of the

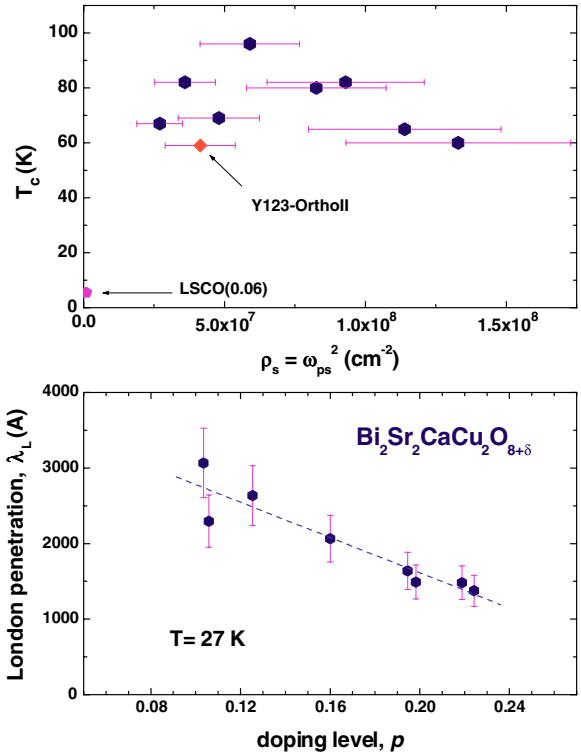

Figure 14. In the upper panel we display T_c versus $\rho_s \equiv \omega_{ps}^2$. We added two data points from underdoped LSCO with $T_c = 5.5$ K and underdoped Y123 in the orthoII phase with $T_c = 59$ K. In the lower panel we display the doping dependent London penetration depth, $\lambda_L(p)$.

normal state, i.e. we extrapolate the temperature dependent trend to get an appropriate normal state $N_{\rm eff}$ at the temperature of the superconducting state considered. Even though the data points do not show a very smooth doping dependence we can clearly observe a crossover from negative (underdoped) to positive (overdoped) kinetic energy change. There is a disagreement on the sign of the kinetic energy change between previous two studies: a negative value for the optimally doped and underdoped Bi-2212 samples was obtained by Molegraaf *et al* [17] and a positive value for optimally doped Bi-2212 was obtained by Boris *et al* [18]. Our result agrees with Molegraaf *et al*. The increasing trend of $\Delta E_{\rm Kin}$ observed here is consistent with results of Deutscher *et al* [19], Gedik *et al* and Carbone *et al* for the same Bi-2212 system. The data of Deutscher *et al* are also shown in the figure.

5. The extended Drude model and the optical self-energy

The extended Drude model offers a detailed description of the charge carrier scattering spectrum and its contribution to the effective mass [34, 96]. In this picture the elastic scattering rate in the Drude expression is allowed to have a frequency dependence and an extra real quantity, $\omega\lambda(\omega)$, is added to the (imaginary) scattering rate. This is necessary to retain the Kramers–Kronig relation between $\sigma_1(\omega)$ and $\sigma_2(\omega)$. In this formalism we can introduce an interesting and useful quantity, the optical self-energy, $\Sigma^{\rm op}(\omega)$, which is closely related to the

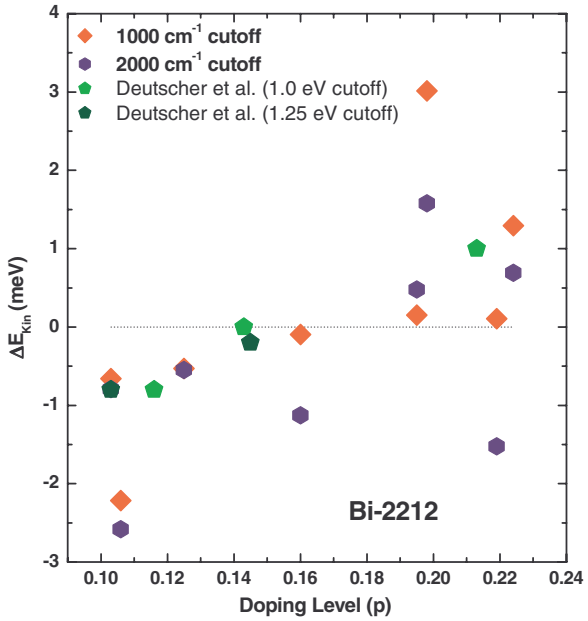

Figure 15. Doping dependent kinetic energy change, $\Delta E_{\mathrm{Kin}} \equiv E^{\mathrm{s}}_{\mathrm{Kin}} - E^{\mathrm{n}}_{\mathrm{Kin}}$, of Bi-2212 when the system becomes a superconductor. We also show data points from Deutscher *et al* for Bi-2212 systems [19].

quasiparticle self-energy [8, 97]:

$$\sigma(\omega, T) = \mathrm{i}\frac{\omega_{\mathrm{p}}^2}{4\pi}\frac{1}{\omega + [\omega\lambda(\omega, T) + \mathrm{i}1/\tau(\omega, T)]} = \mathrm{i}\frac{\omega_{\mathrm{p}}^2}{4\pi}\frac{1}{\omega - 2\Sigma^{\mathrm{op}}(\omega, T)} \tag{18}$$

where ω_{p} is the plasma frequency, $1/\tau(\omega, T)$ is the optical scattering rate, and $\lambda(\omega) + 1 \equiv m^*(\omega)/m$, $m^*(\omega)$ is an effective mass and m is the bare mass. The optical self-energy is a complex function, $\Sigma^{\mathrm{op}}(\omega, T) \equiv \Sigma_1^{\mathrm{op}}(\omega, T) + \mathrm{i}\Sigma_2^{\mathrm{op}}(\omega, T)$, where $-2\Sigma_1^{\mathrm{op}}(\omega, T) = \omega\lambda(\omega, T)$ and $-2\Sigma_2^{\mathrm{op}}(\omega, T) = 1/\tau(\omega, T)$. Σ_1^{op} and Σ_2^{op} make a Kramers–Kronig pair. The optical self-energy contains the plasma frequency, which includes the spectral weight of the free carrier part of the optical conductivity. We obtained the plasma frequency by using a procedure introduced in a previous study [73]. The plasma frequencies are displayed in table 1. The optical self-energy at high frequencies depends strongly on ϵ_{H} (see figure 9 and its caption). The optical self-energy is, apart from a $(\cos\theta - 1)$ factor where θ is a scattering angle, an average over the Fermi surface of the quasiparticle self-energy [7, 8, 98, 99] as measured using angle resolved photoemission spectroscopy (ARPES). ARPES has a capability of k-space resolution while optics has the advantage of better overall energy resolution. The self-energies measured by the two spectroscopy techniques (optical and ARPES) show qualitatively the same properties [8, 35, 39]. However, on a quantitative level there are some fundamental differences between them [97].

Figure 16 displays the optical scattering rates of our eight Bi-2212 samples at various temperatures above and below T_{c}. At room temperature the overall scattering rate decreases

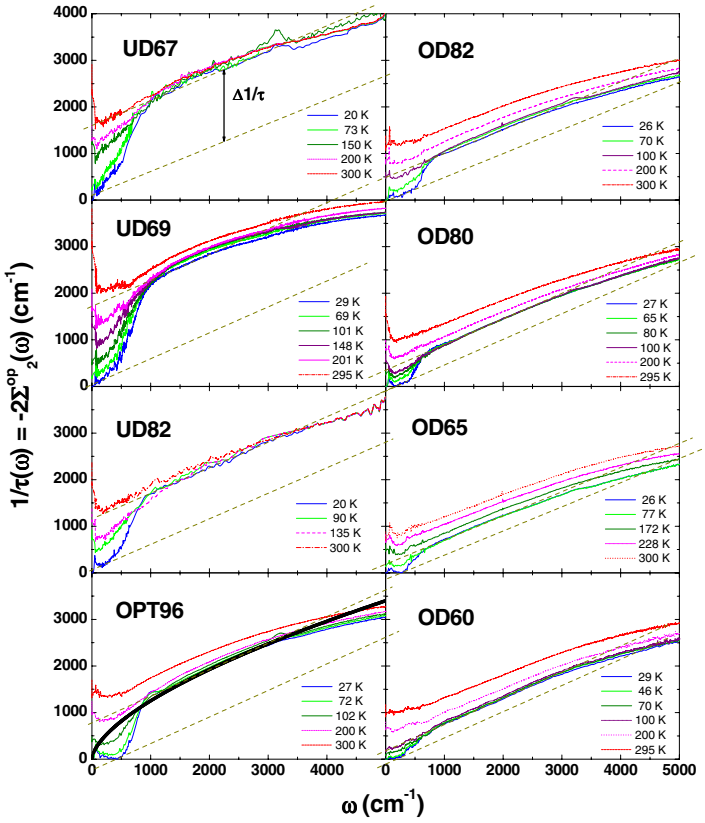

Figure 16. The optical scattering rate or the imaginary part of the optical self-energy of *ab*-plane Bi-2212 at various doping levels and temperatures. $\Delta 1/\tau$ can be a measure of intensity of the step-like feature, which is correlated with the magnetic resonance mode [8, 35, 53]. The intensity of the step shows strong temperature and doping dependences. The thick curve in the panel of OPT96 is $1/\tau(\omega) = 17 \cdot \omega^{2-\gamma}$ where $\gamma = 1.378$ for the optimally doped sample (see the text).

as the doping increases. The scattering rate is fairly linear as a function of frequency up to nearly 3000 cm^{-1} and the slope decreases monotonically with the doping. This linear dependence was described by the phenomenological marginal Fermi liquid theory [62] but we note here that consistently with the power seen in the conductivity, we see a negative curvature in our $1/\tau$ spectra. and we also observe a hint of saturation in the scattering above 3000 cm^{-1}, as suggested by van der Marel *et al* [85]. We add a theoretical scattering curve, $1/\tau(\omega) = \text{constant} \cdot \omega^{2-\gamma}$, in the panel of OPT96 which is obtained using the power law in $\sigma(\omega) = C(\mathrm{i}\omega)^{\gamma-2}$. We note here again the γ is doping dependent (see table 1 and figure 8). At lower temperatures a sharp step-like feature appears in the spectrum. The onset temperature of this feature is higher than T_c for underdoped samples and $\widetilde{=} T_c$ for optimally and overdoped samples. This feature can be fitted with a formalism [53, 100], on the basis of a method proposed by Shulga *et al* [101]. For the fit we need two separate bosonic scattering channels; one is scattering by a sharp mode and the other by a broad background. Hwang *et al* showed that the step-like feature and the sublinear part of the high frequency scattering rate were attributable to the sharp mode and the broad background in the spectral function $\alpha^2 F(\Omega)$, respectively [53]. In the superconducting state we need a formalism that incorporates the superconducting gap

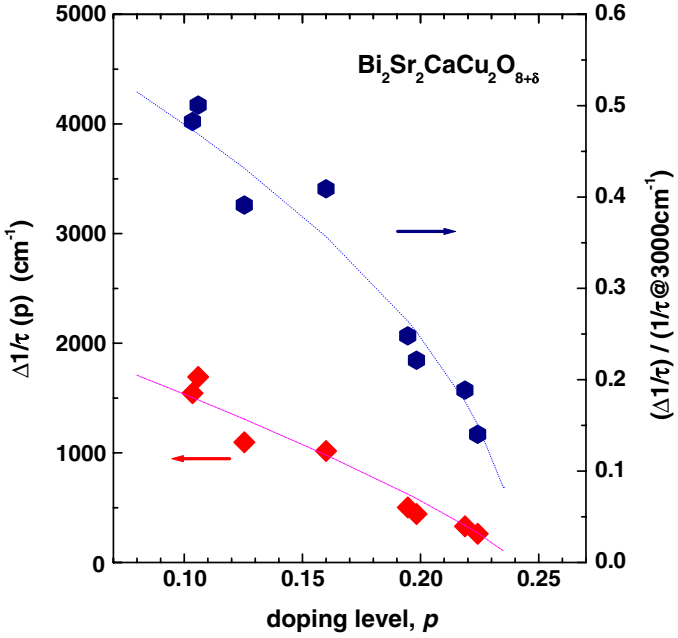

Figure 17. The doping dependent intensity of the step-like feature in the optical scattering rate.

and coherence factors. Qualitatively a similar picture was derived and applied to the optimally doped Bi-2212 system by Schachinger *et al* [98].

We estimate the contribution of the sharp mode to the optical scattering rate by the height of the step in the scattering rate, which is proportional to the area under the mode in the spectral function. We measure the height of the step as follows [8]: we draw a dashed line parallel to the high frequency sublinear trend from an onset point of substantial scattering. The difference between this line and the actual high frequency scattering, $\Delta 1/\tau$ (shown in figure 16), is our estimate of the contribution of the sharp mode to the optical scattering. A doping dependent step intensity, $\Delta 1/\tau(p)$, is shown in figure 17. In the figure we also show a normalized scattering rate, $(\Delta/\tau)/(1/\tau @ 3000\ \mathrm{cm}^{-1})$, divided by the value at 3000 cm^{-1}. The step in intensity decreases rapidly as the doping level increases and becomes zero near a doping level of $p \sim 0.24$ within the superconducting dome, where the superconductivity is still strong in terms of $T_c \sim 55$ K.

In figure 18 we display the real part of the optical self-energy of Bi-2212. This quantity and the scattering rate make a KK pair. At room temperature we see only a very broad background spectrum. The peak frequency of the broad background increases as the doping increases. As the temperature is lowered a well defined sharp peak appears out of the broad room temperature background with the same onset temperature as the step-like feature in the scattering rate and the peak grows as the temperature is reduced further. Johnson *et al* have also resolved a sharp peak and a broad background in ARPES quasiparticle self-energy spectra in the (π, π) direction of Bi-2212 systems and correlated the sharp mode with the magnetic resonance mode of inelastic neutron scattering [42]. More recently similar conclusions have been reached by Kordyuk *et al* [47]. The optical self-energy and ARPES quasiparticle self-energy show strong similarity in terms of their shapes and temperature and doping dependences [8]. Both self-energies have a sharp mode and a broad background at low temperature below T_c while

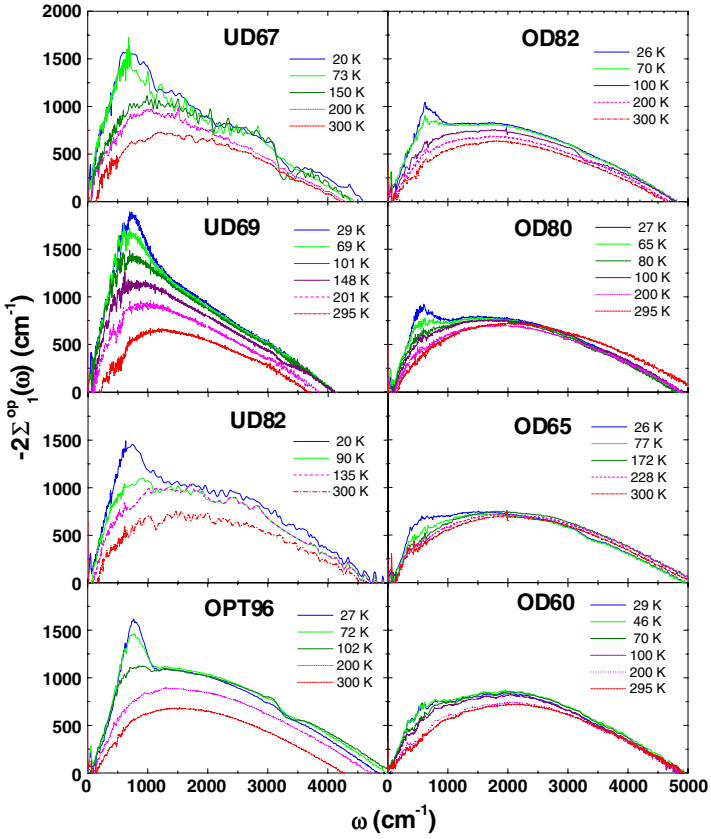

Figure 18. The real part of the optical self-energy of eight Bi-2212 samples at various temperatures. We are able to resolve a sharp peak and a broad background in the spectra. The sharp peak shows strong temperature and doping dependences.

optics shows much better energy resolution. The mode frequencies from the two techniques have an interesting relation: $\Omega_{\text{optical}} \simeq \sqrt{2}\,\Omega_{\text{ARPES}}$, where Ω_{optical} and Ω_{ARPES} are the optical and ARPES mode frequencies, respectively. The relation is consistent with a theoretical prediction [97]. Furthermore Hwang *et al* have analysed the temperature dependent intensity of the step-like feature in the optical scattering rate of orthoII Y123 and found a direct correlation between the step feature in the scattering and the magnetic resonance mode of inelastic neutron scattering (INS) [53].

In the upper panel of figure 19 we show the sharp peak separated from the broad background in the real part of the optical self-energy and we fitted it to a Lorentzian function to obtain the centre frequency, the width, and the height of the peak and the area under it. For the two most underdoped samples it is a little difficult to separate the peak from the broad background because the peak evolves gradually from the broad peak of the background. We display the doping dependent properties of the peak in the lower panel of the figure. The centre frequency (the width) seems to be maximized (minimized) near the optimally doping level. Note that the width does not change much through a wide range of doping. The area and height show a strong doping dependence in the overdoped region; the intensities of both quantities decrease very rapidly as doping increases and finally become zero simultaneously within the

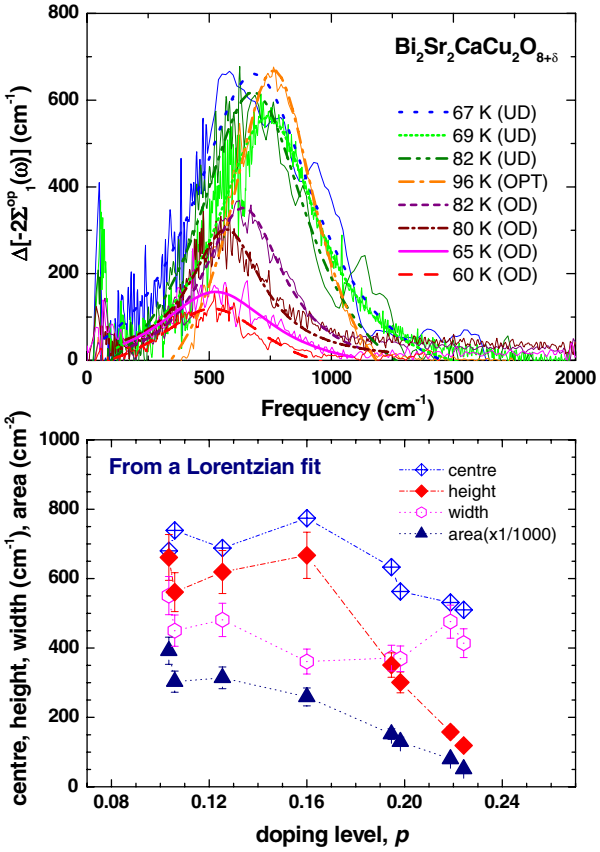

Figure 19. In the upper panel we show the sharp mode separated from the high temperature broad background in the real part of the self-energy and a Lorentzian fit for each doping level. In the lower panel we show the centre frequency, the height, the width of the sharp mode and the area under the mode obtained from the Lorentzian fit.

superconducting dome with a hole doping level, $p \sim 0.24$, estimated from extrapolations. This result is consistent with the doping dependent intensity of the step-like feature in the scattering rate.

For another measure of the strength of the interaction of the charge carriers with the bosonic sharp mode we use the procedure introduced by Marsiglio *et al*, Carbotte *et al*, and Abanov *et al* [35, 102, 103] where the bosonic spectral function, $W(\omega)$, is derived from the second derivative of the optical scattering rate times the frequency. This function can be described as follows [37, 96, 102]:

$$W(\omega) \equiv \frac{1}{2\pi}\frac{\mathrm{d}^2}{\mathrm{d}\omega^2}\left[\frac{\omega}{\tau(\omega)}\right] \tag{19}$$

and $W(\omega) \approx \alpha^2 F(\omega)$ at zero temperature in the normal state, where α is a coupling constant, and $F(\omega)$ is a bosonic density of states. To obtain the spectral function ($W(\omega)$) we followed a smoothing procedure introduced by Tu *et al* [37]. We fit $1/\tau(\omega)$ (see figure 16) with a polynomial with ten terms to catch the main frequency in the spectra without including too much experimental random noise.

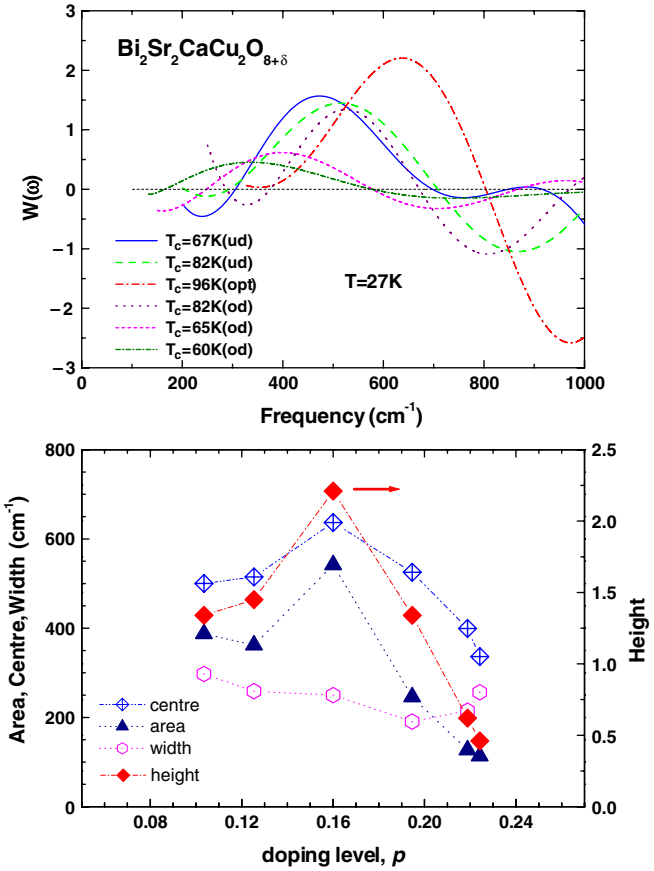

Figure 20. In the upper panel we show the bosonic spectral function, $W(\omega)$, obtained by using the second-derivative formalism (see equation (19)) in the superconducting state, $T \sim 27$ K. We observe a sharp mode in the low frequency range. In the lower panel we show the centre frequency, the height, the width of the sharp mode and the area under the mode in $W(\omega)$.

In the upper panel of figure 20 we show the bosonic spectral function obtained using the second-derivative method, $W(\omega)$ for our six representative Bi-2212 samples at their lowest temperature. In the figure we have subtracted the room temperature background $W(\omega)$ from $W(\omega)$ at the lowest temperature. We should note that the bosonic mode is enhanced in the superconducting state. However, the qualitative doping dependent trend is not affected by the gap [97]. In the lower panel of the figure we display the doping dependent properties of the peak: the centre frequency, the width, and the height of the peak, and the area under the peak. The area is roughly proportional to the quantity $\Delta 1/\tau$ and has the same doping dependent trend as $\Delta 1/\tau$. The extrapolation of the variation with doping of the height and area suggests that the mode will disappear within the superconducting dome in the Bi-2212 phase diagram. The polynomial fit method is fairly robust with respect to experimental noise. We compared this method with alternative methods including an inverse matrix method [104] and found that, for the orthoII material at least, this method gave a well ordered temperature sequence for both the peak position and frequency where alternative methods tended to scramble these quantities.

Since the mode disappears above a critical doping level in the phase diagram leaving the broad background as the only component in the interacting bosonic spectrum it is important

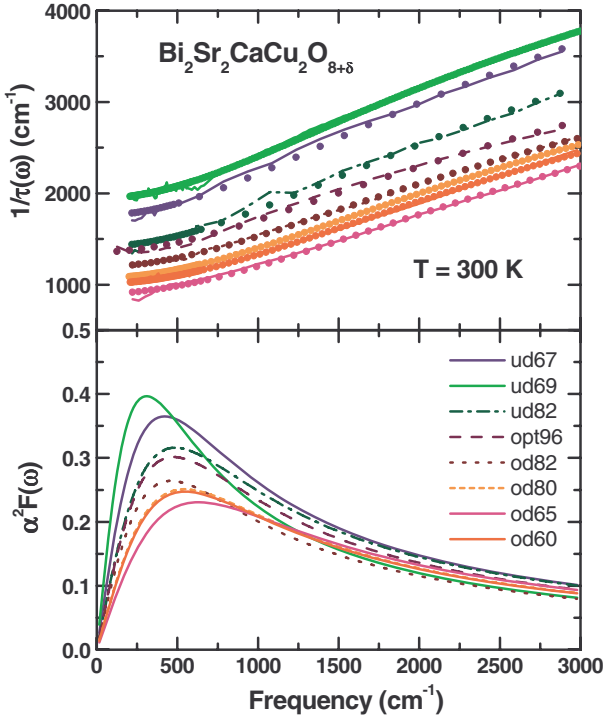

Figure 21. In the upper panel we show the optical scattering rates (lines) of our eight Bi-2212 samples at room temperature and their fits (symbols) obtained by using the methods introduced in the literature [53, 100]. In the lower panel we display the MMP bosonic spectral function, $\alpha^2 F(\omega)$, from the fits in the upper panel.

to investigate this spectrum. We obtained the bosonic spectral functions of our eight Bi-2212 samples by fitting the room temperature scattering rate with the Millis–Monien–Pines (MMP) type of background [24] using the methods introduced by Sharapov *et al* [53, 100]. In the upper panel of figure 21 we show the fits (symbols) and data (lines) for the optical scattering rate. In the lower panel of the figure we display the corresponding bosonic spectral functions. The spectral function shows a slight doping dependence at low frequencies. As we move closer to the antiferromagnetic phase boundary the spectral function grows in strength and develops a more defined peak at low frequency. We also obtain the coupling constant, λ, for this spectrum, which is defined by $\lambda = \int_0^{\omega_c} \alpha^2 F(\omega')/\omega' \, d\omega'$ with $\omega_c = 3000$ cm^{-1}. The resulting doping dependent coupling constant, $\lambda_{BG}(p)$, is shown in figure 22. There is a strong doping dependence in the coupling constant, ranging from 2.25 to 1.25. The value decreases monotonically as doping level increases. This behaviour is not consistent with an observation of Padilla *et al* for LSCO systems [105]: they suggested that there is little doping dependence of the carrier mass which is given by $m^* = m(1 + \lambda)$ across the phase diagram.

6. Discussion and conclusions

6.1. The superfluid density and the kinetic energy change

The doping dependence of the superfluid density in the cuprates has been of great interest from early on when Uemura *et al* found using muon scattering that the superfluid density increases

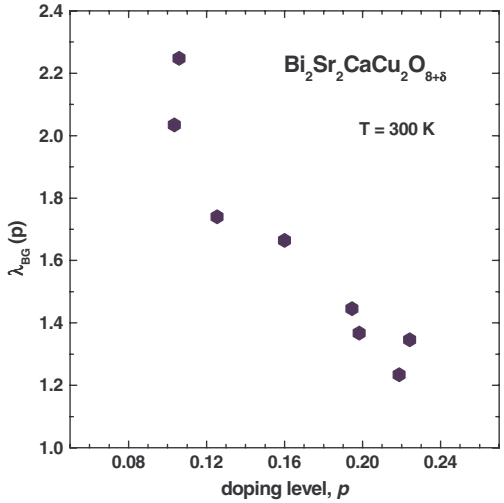

Figure 22. Doping dependent mass enhancement factor, $\lambda(p) = 2\int_0^{\omega_c} \alpha^2 F(\omega')/\omega' \, d\omega'$, where $\omega_c = 3000\ \mathrm{cm}^{-1}$, at room temperature. We used the extracted spectral function, $\alpha^2 F(\omega)$, from the lower panel of figure 21 to get the coupling constant, $\lambda(p)$.

with doping and is proportional to the superconducting transition temperature [106]. This so-called Uemura relationship holds only up to the optimal doping level, at which point T_c stops increasing while the superfluid density continues to increase. There have been reports, for example by Niedermayer *et al* who studied overdoped Tl-based ($Tl_2Ba_2CuO_{6+\delta}$: Tl-2201) cuprates using muon spin resonance, of a so-called boomerang effect where the superfluid density *decreases* in the overdoped region as the doping level *increases* [94]. As we see in figure 14, our data, obtained by two different methods, show that the superfluid density continues to increase in the overdoped region and there is no boomerang effect in this material.

For conventional superconductors the Ferrel–Glover–Tinkham (FGT) sum rule holds. However, the *c*-axis optical transport in the cuprates shows a strong violation of the FGT sum rule which has been attributed to a kinetic energy driven superconductivity [107]. Whether the FGT sum rule holds or not in *ab* optical transport has been the subject of some controversy [17, 18, 108, 109]. Here we find, as shown in figure 15, that a measurable FGT sum rule violation can be observed in *ab*-plane transport of Bi-2212. We do find that we have to take account the temperature dependence of the spectral weight and extrapolate it into the superconducting state. This result is consistent with Deutscher *et al* [19].

6.2. The sharp mode and the broad background in the optical self-energy

We have verified the behaviour of the sharp mode observed by Hwang *et al* [8] over a wide range of dopings with more samples, which is shown in figures 17 and 19, and with a different method of analysis, the second-derivative method, the result of which is shown in figure 20.

We also have studied the broad background in more detail; we extracted doping dependent bosonic spectra shown in figure 21 from room temperature optical scattering rates. The broad peak of the background moves to lower frequencies and its intensity increases as the doping decreases, which is qualitatively consistent with figure 51 of [4]. The coupling constant of the room temperature background, $\lambda_{BG}(p)$, which is displayed in figure 22, decreases significantly as doping increases, which agrees with previous studies [42, 73]. Recently, a new study

has shown that the broad background at room temperature evolves into the sharp mode with lowering temperature and this temperature evolution shows strong doping dependence [110].

6.3. Summary and conclusion

We obtained the superfluid density with two different methods from our ab-plane optical conductivity and observed that the superfluid density increased monotonically with the hole doping level. The smooth and monotonic increase of the superfluid density with the doping supports the overall consistency of our study. We took into account the temperature dependence in the optical spectral weight for extracting the superfluid density and observed a violation of the FGT sum rule, the result of which causes a change of the kinetic energy of the charge carriers at the superconducting transition. Kinetic energy increases (decreases) in overdoped (underdoped) systems as the system becomes a superconductor. We also confirmed our previous work [8] with more samples and a different method of analysis. We resolved a sharp mode out of a broad background in the optical self-energy. The temperature and doping dependence of the sharp mode is dramatic; the onset temperature T_s of the sharp mode is above (at) T_c in underdoped (overdoped) systems and the intensity of the mode gets weakened strongly in the overdoped region with increasing doping, and an extrapolation of the doping trend shows a complete disappearance above a critical doping, $p_c \sim 0.24$, within the superconducting dome. The broad background is present at all temperatures and doping levels and shows relatively weak doping and temperature dependence. However the coupling constant of the background decreases measurably as the doping increases.

Acknowledgments

This work was supported by the Canadian Natural Science and Engineering Research Council and the Canadian Institute of Advanced Research. The work at Brookhaven was supported in part by the Department of Energy. We thank J P Carbotte for giving helpful and thoughtful comments. We thank H Eisaki and M Greven for supplying us with several crystals. Their work at Stanford University was supported by the Department of Energy's Office of Basic Sciences, Division of Materials Science.

References

[1] Bednorz T G and Müller K A 1986 *Z. Phys.* B **64** 189
[2] Carbotte J P 1990 *Rev. Mod. Phys.* **62** 1027
[3] McMillan W L and Rowell J M 1969 *Superconductivity* vol 1, ed R D Parks (New York: Dekker) p 561
[4] Eschrig M 2006 *Adv. Phys.* **55** 47
[5] Damascelli A, Hussain Z and Shen Z-X 2003 *Rev. Mod. Phys.* **75** 473
[6] Mourachkine A 2005 *Mod. Phys. Lett.* B **19** 743
[7] Kaminski A *et al* 2000 *Phys. Rev. Lett.* **84** 1788
[8] Hwang J, Timusk T and Gu G D 2004 *Nature* **427** 714
[9] Basov D N and Timusk T 2005 *Rev. Mod. Phys.* **77** 721
[10] Puchkov A V, Fournier P, Basov D N, Timusk T, Kapitulnik A and Kolesnikov N N 1996 *Phys. Rev. Lett.* **77** 3212
[11] Puchkov A V, Basov D N and Timusk T 1996 *J. Phys.: Condens. Matter* **8** 10049
[12] Quijada M A, Tanner D B, Kelley R J, Onellion M, Berger H and Margaritondo G 1999 *Phys. Rev.* B **60** 14917
[13] Liu H L *et al* 1999 *J. Phys.: Condens. Matter* **11** 239
[14] Ferrell R A and Glover R E III 1956 *Phys. Rev.* **109** 1398
Glover R E III and Tinkham M 1956 *Phys. Rev.* **104** 844
Glover R E III and Tinkham M 1957 *Phys. Rev.* **108** 243

[15] Hirsch J 1992 *Physica* C **199** 305
[16] Hirsch J and Marsiglio F 2000 *Phys. Rev.* B **62** 15131
[17] Molegraaf H J A, Presura C, van der Marel D, Kes P H and Li M 2002 *Science* **295** 2239
[18] Boris A V, Kovaleva N N, Dolgov O V, Holden T, Lin C T, Keimer B and Bernhard C 2004 *Science* **304** 708
[19] Deutscher G, Santander-Syro A F and Bontemps N 2005 *Phys. Rev.* B **72** 092504
[20] Gedik N, Langner M, Orenstein J, Ono S, Abe Y and Ando Y 2005 *Phys. Rev. Lett.* **95** 117005
[21] Carbone F *et al* 2006 *Phys. Rev.* B **74** 064510
[22] Carbotte J P and Schachinger E 2006 *Preprint* cond-mat/0608116
[23] Monthoux P, Balatsky A V and Pines D 1991 *Phys. Rev. Lett.* **67** 3448
[24] Millis A J, Monien H and Pines D 1990 *Phys. Rev.* B **42** 167
[25] Rossat-Mignod J, Regnault L P, Vettier C, Bourges P, Burlet P, Bossy J, Henry J Y and Lapertout G 1991 *Physica* C **185–189** 86
[26] Mook H A, Yethiraj M, Aeppli G, Mason T E and Armstrong T 1993 *Phys. Rev. Lett.* **70** 3490
[27] Fong H F, Keimer B, Anderson P W, Reznik D, Dogan F and Aksay I A 1995 *Phys. Rev. Lett.* **75** 316
[28] Mook H A, Dai P, Hayden S M, Aeppli G, Perring T G and Dogan F 1998 *Nature* **395** 580
[29] Dai P, Mook H A, Hayden S M, Aeppli G, Perring T G, Hunt R D and Doan F 1999 *Science* **284** 1344
[30] Fong H F, Bourges P, Sidis Y, Regnault L P, Ivanov A, Gu G D, Koshizuka N and Keimer B 1999 *Nature* **398** 588
[31] He H *et al* 2001 *Phys. Rev. Lett.* **86** 1610
[32] He H, Bourges P, Sidis Y, Ulrich C, Regnault L P, Pailhes S, Berzigiarova N S, Kolesnikov N N and Keimer B 2002 *Science* **295** 1045
[33] Thomas G A, Orenstein J, Rapkine D H, Capizzi M, Millis A J, Bhatt R N, Schneemeyer L F and Waszczak J V 1988 *Phys. Rev. Lett.* **61** 1313
[34] Puchkov A V, Basov D N and Timusk T 1996 *J. Phys.: Condens. Matter* **8** 10049
[35] Carbotte J P, Schachinger E and Basov D N 1999 *Nature* **401** 354
[36] Abanov Ar and Chubukov A V 1999 *Phys. Rev. Lett.* **83** 1652
[37] Tu J J, Homes C C, Gu G D, Basov D N and Strongin M 2002 *Phys. Rev.* B **66** 144514
[38] Shen Z-X and Schrieffer J R 1997 *Phys. Rev. Lett.* **78** 1771
[39] Norman M R and Ding H 1998 *Phys. Rev.* B **57** R11089
[40] Campuzano J C *et al* 1999 *Phys. Rev. Lett.* **83** 3709
[41] Bogdanov P V *et al* 2000 *Phys. Rev. Lett.* **85** 2581
[42] Johnson P D *et al* 2001 *Phys. Rev. Lett.* **87** 177007
[43] Kaminski A, Randeria M, Campuzano J C, Norman M R, Fretwell H, Mesot J, Sato T, Takahashi T and Kadowaki K 2001 *Phys. Rev. Lett.* **86** 1070
[44] Zasadzinski J F, Ozyuzer L, Miyakawa N, Gray K E, Hinks D G and Kendziora C 2001 *Phys. Rev. Lett.* **87** 067005
[45] Zasadzinski J F, Ozyuzer L, Coffey L, Gray K E, Hinks G D and Kendziora C 2006 *Phys. Rev. Lett.* **96** 017004
[46] Stock C, Buyers W J L, Liang R, Peets D, Tun Z, Bonn D, Hardy W N and Birgeneau R J 2004 *Phys. Rev.* B **69** 014502
[47] Kordyuk A A *et al* 2005 *Preprint* cond-mat/0510760
[48] Demler E and Zhang Z C 1998 *Nature* **396** 733
[49] Scalapino D J 1999 *Science* **284** 1282
[50] Kee H-Y, Kivelson S A and Aeppli G 2002 *Phys. Rev. Lett.* **88** 257002 and references therein
[51] Munzar D, Bernhard C and Cardona M 1999 *Physica* C **317/318** 547
[52] Abanov Ar, Chubukov A V, Eschrig M, Norman M R and Schmalian J 2002 *Phys. Rev. Lett.* **89** 177002
[53] Hwang J, Yang J, Timusk T, Sharapov S G, Carbotte J P, Bonn D A, Liang R and Hardy W N 2006 *Phys. Rev.* B **73** 014508
[54] Ma Y C and Wang N L 2006 *Phys. Rev.* B **73** 144503
[55] Shibauchi T, Krusin-Elbaum L, Li M, Maley M P and Kes P H 2001 *Phys. Rev. Lett.* **86** 5763
[56] Ozyuzer L, Zasadzinski J F, Gary K E, Kendziora C and Miyakawa N 2002 *Europhys. Lett.* **58** 589
[57] Yoshida T *et al* 2001 *Phys. Rev.* B **63** 220501
[58] Takeuchi T, Yokoya T, Shin S, Jinno K, Matsuura M, Kondo T, Ikuta H and Mizutani U 2001 *J Electron Spectrosc. Relat. Phenom.* **114–116** 629
[59] Ino A, Kim C, Nakamura M, Yoshida T, Mizokawa T, Fujimori A, Shen Z-X, Kakeshita T, Eisaki H and Uchida S 2002 *Phys. Rev.* B **65** 094504
[60] Kaminski A, Rosenkranz S, Fretwell H M, Norman M R, Randeria M, Campuzano J C, Park J-M, Li Z Z and Raffy H 2006 *Phys. Rev.* B **73** 174511

[61] Takeuchi T, Kondo T, Kitao T, Kaga H, Yang H, Ding H, Kaminski A and Campuzano J C 2005 *Phys. Rev. Lett.* **95** 227004
[62] Varma C M, Littlewood P B and Schmitt-Rink S 1989 *Phys. Rev. Lett.* **63** 1996
[63] Hayden S M, Aeppli G, Dai P, Mook H A, Perring T G, Cheong S-W, Fisk Z, Doan F and Mason T E 1998 *Physica* B **241–243** 765
[64] Lanzara A *et al* 2001 *Nature* **412** 510
[65] Hwang J, Yang J, Timusk T and Chou F C 2005 *Phys. Rev.* B **72** 024549
[66] Collins R T, Schlesinger Z, Holtzberg F, Chaudhari P and Feild C 1989 *Phys. Rev.* B **39** 6571
[67] Eisaki H, Kaneko M, Feng D L, Damascelli A, Mang P K, Shen K M, Shen Z-X and Greven M 2004 *Phys. Rev.* B **69** 064512
[68] Orenstein J and Rapkine D H 1988 *Phys. Rev. Lett.* **60** 968
[69] Reedyk M and Timusk T 1992 *Phys. Rev. Lett.* **69** 2705
[70] Hwang J, Sills K and Timusk T 2003 unpublished
[71] Homes C C, Reedyk M A, Crandles D A and Timusk T 1993 *Appl. Opt.* **32** 2976
[72] Presland M R, Tallon J L, Buckley R G, Liu R S and Flower N E 1991 *Physica* C **176** 95
[73] Hwang J, Timusk T, Puchkov A V, Wang N L, Gu G D, Homes C C, Tu J J and Eisaki H 2004 *Phys. Rev.* B **69** 094520
[74] Wooten F 1972 *Optical Properties of Solids* (New York: Academic)
[75] Santander-Syro A F, Lobo R P S M, Bontemps N, Konstantinovic Z, Li Z and Raffy H 2002 *Phys. Rev. Lett.* **88** 097005
[76] Kuzmenko A B 2005 *Rev. Sci. Instrum.* **76** 083108
[77] Terasaki I, Tajima S, Eisaki H, Takagi H, Uchinokura K and Uchida S 1990 *Phys. Rev.* B **41** 865
[78] Mattis D C and Bardeen J 1958 *Phys. Rev.* **111** 412
[79] Tinkham M 1975 *Introduction to Superconductivity* (New York: McGraw-Hill)
[80] Leplae L 1983 *Phys. Rev.* B **27** 1191
[81] Zimmermann W, Brandt E H, Bauer M, Seider E and Genzel E 1991 *Physica* C **183** 99
[82] Takenaka K, Mizuhashi K, Takagi H and Uchida S 1994 *Phys. Rev.* B **50** 6534
[83] Sutherland M L 2004 *Thesis* University of Toronto
[84] Anderson P W 1997 *Phys. Rev.* B **55** 11785
[85] van der Marel D, Molegraaf H J A, Zaanen J, Nussinov Z, Carbone F, Damascelli A, Eisaki H, Greven M, Kes P H and Li M 2003 *Nature* **425** 271
[86] Anderson P W 2005 *Preprint* cond-mat/0512471
[87] Basov D N, Puchkov A V, Hughes R A, Strach T, Preston J, Timusk T, Bonn D A, Liang R and Hardy W N 1994 *Phys. Rev.* B **49** 12165
[88] Carbone F, Kuzmenko A B, Molegraaf H J A, van Heumen E, Giannini E and van der Marel D 2006 *Phys. Rev.* B **74** 024502
[89] Ortolani M, Calvani P and Lupi S 2005 *Phys. Rev. Lett.* **94** 067002
[90] Bontemps N 2006 *Preprint* cond-mat/0610307
[91] Dordevic S V, Singley E J, Basov D N, Komiya S, Ando Y, Bucher E, Homes C C and Strongin M 2002 *Phys. Rev.* B **65** 134511
[92] Norman M and Pépin C 2003 *Rep. Prog. Phys.* **66** 1547
[93] Homes C C, Dordevic S V, Bonn D A, Liang R and Hardy W N 2004 *Phys. Rev.* B **69** 024514
[94] Niedermayer Ch, Bernhard C, Binninger U, Glückler H, Tallon J L, Ansaldo E J and Budnick J I 1993 *Phys. Rev. Lett.* **71** 1764
[95] Villard G, Pelloquin D and Maignan A 1998 *Phys. Rev.* B **58** 15231 and references therein
[96] Allen P B 1971 *Phys. Rev.* B **3** 305
[97] Carbotte J P, Schachinger E and Hwang J 2005 *Phys. Rev.* B **71** 054506
[98] Schachinger E, Tu J J and Carbotte J P 2003 *Phys. Rev.* B **67** 214508
[99] Millis A J and Drew H D 2003 *Phys. Rev.* B **67** 214517
[100] Sharapov S G and Carbotte J P 2005 *Phys. Rev.* B **72** 134506
[101] Shulga S V, Dolgov O V and Maksimov E G 1991 *Physica* C **178** 266
[102] Marsiglio F, Startseva T and Carbotte J P 1998 *Phys. Lett.* A **245** 172
[103] Abanov A, Chubukov A V and Schmalian J 2001 *Phys. Rev.* B **63** 180510(R)
[104] Dordevic S V, Homes C C, Tu J J, Valla T, Strongin M, Johnson P D, Gu G D and Basov D N 2005 *Phys. Rev.* B **71** 104529
[105] Padilla W J, Lee Y S, Dumm M, Blumberg G, Ono S, Segawa K, Komiya S and Ando Y 2005 *Phys. Rev.* B **72** 060511
[106] Uemura Y J *et al* 1991 *Phys. Rev. Lett.* **66** 2665

[107] Basov D N, Woods S I, Katz A S, Singley E J, Dynes R C, Xu M, Hinks D G, Homes C C and Strongin M 1999 *Science* **283** 49
[108] Kuzmenko A B, Molegraaf H J A, Carbone F and van der Marel D 2005 *Phys. Rev.* B **72** 144503
[109] Santander-Syro A F, Lobo R P S M, Bontemps N, Lopera W, Giratá D, Konstantinovic Z, Li Z Z and Raffy H 2004 *Phys. Rev.* B **70** 134504
[110] Hwang J, Timusk J, Schachinger E and Carbotte J P 2006 *Preprint* cond-mat/0610127